7-2014

Effect of Evaporation Momentum Force on a Bubble Under Asymmetric Temperature Conditions

Pruthvik A. Raghupathi

R·I·T | KATE GLEASON *College of* ENGINEERING

EFFECT OF EVAPORATION MOMENTUM FORCE ON A BUBBLE UNDER ASYMMETRIC TEMPERATURE CONDTIONS

by

Pruthvik A. Raghupathi

A Thesis Submitted in Partial Fulfillment of the Requirements for the Degree of

MASTER OF SCIENCE

in

MECHANICAL ENGINEERING

DEPARTMENT OF MECHANICAL ENGINEERING

KATE GLEASON COLLEGE OF ENGINEERING

ROCHESTER INSTITUTE OF TECHNOLOGY

ROCHESTER, NY 14623

JULY 2014

Approved by:

_____ _____

Dr. Satish G. Kandlikar Date

Thesis Advisor

Professor, Department of Mechanical Engineering

_____ _____

Dr. Robert J. Stevens Date

Committee Member

Professor, Department of Mechanical Engineering

_____ _____

Dr. Mario W. Gomes Date

Committee Member

Professor, Department of Mechanical Engineering

_____ _____

Dr. Agamemnon Crassidis Date

Department Representative

Professor, Department of Mechanical Engineering

Abstract

Boiling has for a long time been regarded as a promising option in a wide range of applications such as electronic cooling, steam generation in boiler or solar concentrators, space applications etc. In order to make boiling a more attractive option for various applications many surface enhancements have been developed to improve the heat transfer performance during boiling. Recent literature indicates that boiling performance can be significantly improved by using evaporation momentum force to control the trajectory of a bubble. This approach merits a detailed investigation into evaporation momentum force, its effect on bubble growth, bubble trajectory and heat transfer. The objective of the current work is to theoretically determine and experimentally observe the effect of evaporation momentum force on the trajectory of a bubble.

An expression for evaporation momentum pressure resulting from the evaporation momentum force experienced by a bubble is determined. The expression is incorporated into a well established bubble growth models to evaluate the effect of evaporation momentum pressure on bubble growth rate. The effect of evaporation momentum force on a bubble growing in asymmetric temperature field is then studied and the resultant trajectory is evaluated. The results are compared with experimental data of bubble trajectory subjected to an asymmetric temperature condition obtained using a high speed camera. The final results suggest that the evaporation momentum pressure in the vicinity of contact line can significantly change the bubble trajectory, and surfaces designed to exploit this effect seem to be promising for boiling enhancement.

Acknowledgements

I would firstly like to express gratitude to my advisor Dr. Satish Kandlikar for giving me an opportunity to work under his guidance in the Thermal Analysis, Microfludics and Fuel Cell Lab. His support and encouragement throughout the project was crucial to make this project a reality.

I would like to thank Dr. Robert Stevens, Dr. Mario Gomes and Dr. Agamemnon Crassidis for their feedback and encouragement. I am grateful to Dr. Surendra Gupta for giving access to the polishing equipment whenever needed.

I am thankful to all the past and present members of the Thermal Analysis, Microfludics and Fuel Cell Lab for backing me whenever I was in doubt and for making my stay at the lab an enjoyable one.

I am grateful to the National Science Foundation for providing financial aid under Award No. 1335927.

Finally I would like to thank my parents, sister and family for their love, encouragement and support throughout my life. They have been a source of strength all my life and I owe everything to them.

Contents

List of Figures

List of Tables

Nomenclature

A	Parameter defined by Mikic
B	Parameter defined by Mikic
c	Coefficient of proportionality defined by Eq. 27
C_D	2D Coefficient of Drag
F_M	Evaporation momentum force (N)
F_S	Surface tension force (N)
F_G	Hydraulic force (N)
H	Bubble height (m)
Ja	Jacob number
P	Pressure ($kg\ m/s^2$)
R	Bubble radius (m)
Re	Reynolds Number
T	Temperature (K)
V	Velocity (m/s)
a_l	Thermal diffusivity
b	Shape factor
h	Enthalpy (kJ/Kg)
q	Heat flux (W/m^2)
u	Liquid velocity (m/s)
$\dot{m}$	Rate of change of mass (kg/s)
$\dot{R}$	Bubble growth rate (m/s)

δ	Thermal boundary thickness (m)
η	Mass flux ($\frac{\mathrm{kg}}{\mathrm{m^2 s}}$)
ρ	Density ($\frac{kg}{m^3}$)
σ	Surface tension ($\frac{N}{m}$)
μ	Dynamic viscosity $\left(\frac{N-s}{m^2}\right)$
ϑ	Kinematic Viscosity $\left(\frac{m^2}{s}\right)$
θ_c	Contact angle
φ	Angle corresponding to boundary layer thickness
$()_l$	Liquid
$()_v$	Vapor
$()_I$	Interface

1.0 INTRODUCTION

One of the current thrust areas in the field of thermal engineering is the thermal management of electronic devices. Over the past few years, the number of components present in electronic devices has increased exponentially. In the process of making electronic devices more powerful the number of transistors present in a chip is doubling every 18 months and the distance between transistors is also steadily reducing so that the latency in the devices reduces. As a result of these improvements the amount of heat produced in a given area is set to increase dramatically. Transistor devises are thermally sensitive and are susceptible to failure or reduced performance if the temperature goes beyond 85^{o}C. Therefore a need exists for reliable and efficient cooling solutions to regulate the temperature of the devices. Currently, low power devices are air cooled while high performance systems like those used in large servers, data centers and supercomputers are liquid cooled. Table 1 shows the heat transfer coefficients observed for popular cooling methods.

Process	**Fluid**	**Heat transfer coefficient (W/m^2-K)**
Natural convection	Air	2-25
	Water	50-1000
Forced convection	Air	25-250
	Water	100-20,000
Pool boiling	Fluorochemicals	1000-50,000
	Water	2500-100,000

Table 1: Heat transfer coefficient for different modes of heat transfer

1.1 Boiling

Since the latent heat of liquid is always significantly greater than the specific/sensible heat of the liquid, heat transfer due to phase change is substantially higher than single phase heat transfer. Boiling is a heat transfer process accompanied by phase change from liquid to vapor. It is further classified into pool and flow boiling. Pool boiling is the boiling of a stagnant liquid over a heated surface while flow boiling is the boiling of a flowing fluid over a heated surface. In case of pool boiling the growth and departure of bubbles is the main reason for liquid motion while in case of flow boiling the presence of an external force also aids in the mixing of the liquid. While flow boiling can result in high heat transfer, inherent difficulties such as flow instability and large power requirement to pump or high pressure drop make its use difficult in certain applications.

1.2 Pool boiling

Pool boiling is a mode of heat transfer where a heated surface is submerged in a pool of stagnant liquid and phase change occurs on top of the heated surface. Unlike flow boiling or other forced convection methods, there are no moving parts in a pool boiling setup and hence the system is relatively very simple and inexpensive. Since liquid circulation does not occur, almost all of the heat absorbed by the fluid is towards latent heat of the liquid. Boiling applications include boilers parabolic solar concentrators, heat exchangers etc. current research is pool boiling aims to improve the maximum heat flux which the system can handle and the heat transfer coefficient of the system.

1.3 Boiling curve

Boiling curve is a graph showing the variation of surface temperature at different heat fluxes. The different mechanisms observed during boiling can be clearly differentiated in a boiling

curve. Fig. 1 shows a generic pool boiling curve for a liquid on a heated surface. The curve is divided into four regimes:

i) Natural convection

ii) Nucleate boiling

iii) Transition boiling

iv) Film boiling

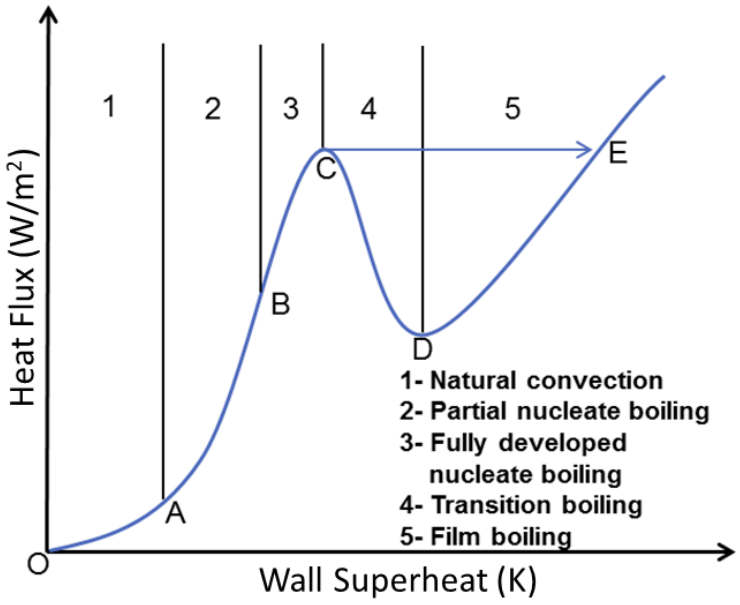

Figure 1: General Pool boiling curve

1.3.1 Free convection

Free convection is the first regime of heat transfer in boiling and is observed between points O and A in Fig. 1. In this region, despite the wall superheat being above the saturation temperature, boiling is not observed as at low wall superheats the temperature of the liquid in the thermal boundary layer is not enough to initiate or sustain bubble nucleation. Boiling is first observed at point A and is referred to as Onset of Nucleate Boiling (ONB).

1.3.2 Nucleate boiling

The nucleate boiling regime begins at ONB when the first bubble nucleates on the heater surface. After the first bubble has nucleated, many more cavities on the surface of the heater are activated and boiling is observed throughout the surface of the heater. A sudden temperature drop is sometimes observed at ONB due to the nucleation of bubbles from many cavities on the surface. Between ONB and point B partial nucleate boiling is said to occur. During partial nucleate boiling, nucleation is observed at distinct locations on the heater surface and there is little interaction between bubbles at different cavities.

As the heat flux increases the number of active sites also increases and soon bubbles from neighboring cavities begin to coalesce and vapor columns or vapor jets are formed. This phase, which is observed between points B and C, is called fully developed nucleate boiling. During fully developed nucleate boiling, a point of inflection is observed and at this point the heat transfer coefficient is highest.

When the heat flux at the surface is further increased, the interaction between neighboring bubbles also increases. At point C, the maximum heat flux possible during nucleate boiling, which is known as the Critical Heat Flux (CHF) is reached. At CHF a thin layer of vapor covers the heater surface and prevents the liquid from touching the heater surface. The layer of vapor drastically reduces the heat transfer coefficient of the surface and hence the temperature of the heater rises almost instantaneously and the system moves from point C to point E.

1.3.3 Transition boiling

After reaching CHF the boiling mechanism instantly changes from fully developed nucleate boiling to film boiling. The change is accompanied by a sudden rise in temperature as show by

the line CE in Fig. 1. However, in a temperature controlled system since a sudden spike in temperature is not possible the heat flux drops till point D is reached and is called the Leidenfrost point. Between points C and D an unstable vapor layer is established on the surface thereby reducing the heat transferred across the surface. After point D the vapor film becomes stable and hence the heat transfer rate begins to increase.

1.3.4 Film boiling

Upon formation of a stable film layer the boiling regime changes from transition boiling to film boiling. In case of a heat flux controlled system, film boiling is observed immediately after CHF is reached without traversing the transition boiling region. Since the surface is completely covered by a layer of vapor all the heat is transferred through the layer of vapor and hence the heat transfer coefficient is very low. Since most systems cannot handle the high temperatures associated with film boiling they are maintained below CHF in the nucleate boiling regime.

2.0 LITERATURE REVIEW

2.1 Bubble nucleation

Boiling occurs on specific sites on the heater surface which are referred to as nucleation sites. Nucleation sites are generally cavities containing a small pocket of air or vapor. A schematic of a bubble growing on such a cavity and the temperature profile of the liquid surrounding the bubble is shown in Fig. 2.

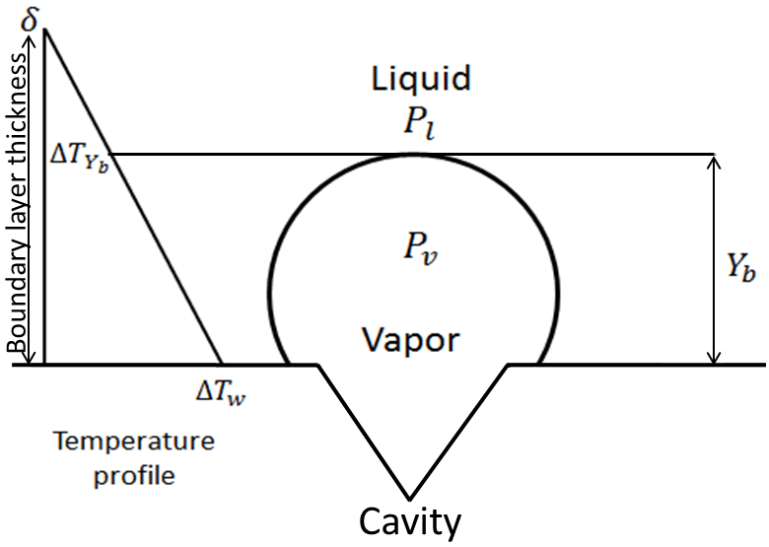

Figure 2: Schematic of bubble nucleation and temperature profile

The liquid on top of the heater surface gets heated beyond saturation temperature and a thermal boundary layer is formed. For bubble nucleation to occur, the temperature of the liquid surrounding the cavity must be greater than the saturation temperature corresponding to the pressure of the air pocket. The pressure of the vapor inside the bubble is considerably higher than the liquid pressure due to surface tension of the liquid acting on the bubble. Mathematically the vapor pressure inside a bubble of radius *R* is given by Eq. 1.

$$P_v - P_l = \frac{2\sigma}{R} \quad (1)$$

Since the temperature of the liquid at the top of the bubble is the lowest, for the bubble to grow the temperature of the liquid at the top of the bubble must be higher than saturation temperature corresponding to the pressure in the bubble.

2.2 Modes of heat transfer

The principle modes of heat transfer that have been proposed are:

i) Transient conduction

Mikic and Rohsenow [1] suggested that the principle mechanism of heat transfer during boiling is transient conduction due to which the liquid above the heater surface is superheated. As the bubble departs the superheated liquid is pumped away from the heater surface and saturated bulk liquid replaces it.

ii) Transient convection/micro convection

Rohsenow [2] developed a model which claimed that convection is the principle mechanism of heat transfer during boiling. The agitation due to bubble growth and departure causes turbulence which in turn increases heat transfer.

iii) Microlayer evaporation

Snyder and Edwards [3] first proposed microlayer evaporation as a major contributing factor during boiling. Later on, Cooper and Lloyd [4] obtained temperature measurements of the heater surface to quantify the effect of microlayer evaporation.

In both the transient conduction and transient convection modes, heat is transferred from the heater to the liquid and evaporation takes place at the liquid vapor interface. While the microlayer evaporation accounts for about 20% of the total heat transferred, most of this takes

place at the three-phase line and hence it can be concluded that most of the phase change from liquid to vapor occurs at the liquid vapor interface [5].

2.3 Bubble growth rate

Through the life of a bubble the rate of bubble growth varies significantly. Fig.3 shows a generic graph of variation of bubble radius with time.

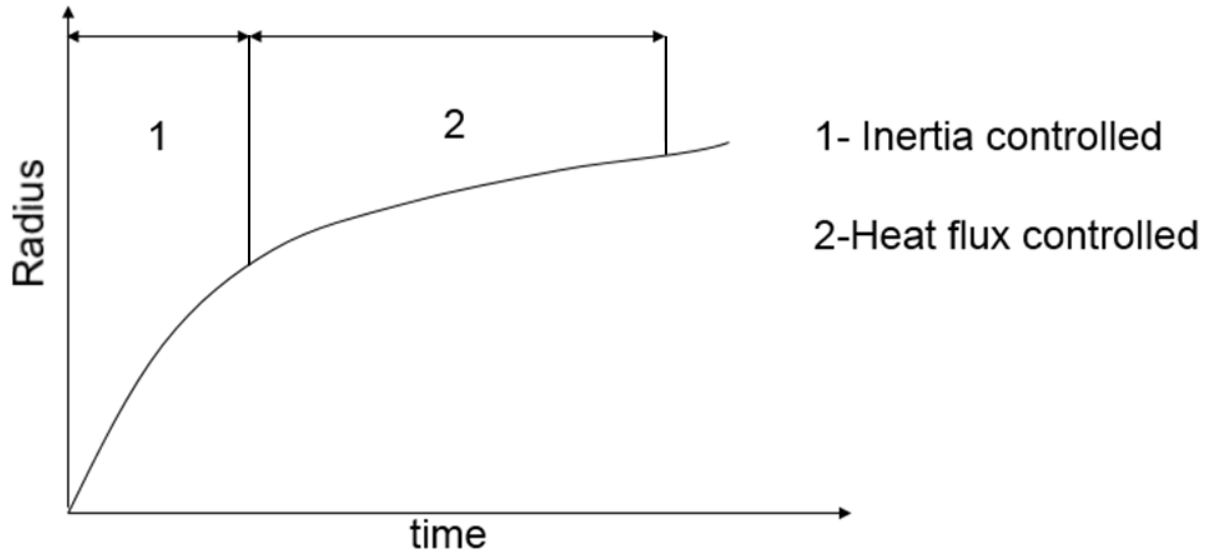

Figure 3: Variation of bubble growth rate

The growth of a bubble can be divided into two phases:

i) Inertia controlled: In the initial stages of a bubble the limiting factor for bubble growth is the displacement of the liquid around the bubble. Since a small amount of vapor is required to increase the radius of the bubble the rate of bubble growth is very high. This phase of bubble growth can be predicted using Rayleigh's [6] model.

ii) Thermally controlled: As the bubble becomes bigger the amount of vapor required to increase the radius of the bubble also increases. Also, due to evaporation the superheat of the liquid around the bubble also decreases. Therefore, the rate at which

the bubble grows reduces. This phase of bubble growth is modeled by Plesset and Zwick [7]

Over the years several models have been proposed which predict bubble growth under various conditions. Some of the widely used models which predict bubble growth are:

Rayleigh-Plesset model

The Rayleigh Plesset equation is an ordinary differential equation which describes the growth of a spherical bubble in an infinite body of liquid. It was developed to model liquid cavitation and hence does not include any heat transfer term. Since the initial phase of bubble growth is inertia controlled, Rayleigh-Plesset equation can be used to model the initial stage of a bubble .

For a bubble growing in an infinite body of liquid, the velocity of the liquid at a point, *u(r, t)* is given by:

$$u(r,t) = \frac{R^2}{r^2}\frac{dR}{dt} \tag{2}$$

Where *R* is the radius of the bubble. Navier-Stokes equation in spherical coordinates is given by

$$\rho_l\left(\frac{\partial u}{dt} + u\frac{\partial u}{dr}\right) = -\frac{\partial P}{\partial R} + \mu_l\left(\frac{1}{r^2}\frac{\partial}{\partial r}\left(r^2\frac{\partial u}{\partial r}\right) - \frac{2u}{r^2}\right) \tag{3}$$

Substituting Eq. 2 in Eq. 3 and integrating from *r*=*R* to *r*=∞, Eq. 4 is obtained,

$$\frac{P(R)-P(\infty)}{\rho_l} = R\frac{d^2R}{dt^2} + \frac{3}{2}\left(\frac{dR}{dt}\right)^2 \tag{4}$$

Applying the boundary conditions the term *P(R)* can be written as,

$$P(R) = -\frac{4\mu_l}{R}\frac{dR}{dt} - \frac{2\sigma}{R} + P_v \tag{5}$$

Where P_v is the vapor pressure inside the bubble. Combining Eq. 4 and Eq. 5 the final form of the equation is obtained as shown in Eq. 6.

$$\frac{P_v - P_l}{\rho_l} = R\frac{d^2R}{dt^2} + \frac{3}{2}\left(\frac{dR}{dt}\right)^2 + \frac{4\vartheta_l}{R}\frac{dR}{dt} + \frac{2\sigma}{\rho_l R} \tag{6}$$

Strutt [6] first derived the equation without considering the effects of surface tension and viscosity and Plesset [8] later modified the equation to account for viscous forces due to liquid displacement and surface tension changes.

Plesset and Zwick model [7]

As the bubble grows past the inertia controlled growth phase the transfer of heat from the liquid surrounding the bubble becomes the limiting factor for bubble growth. By solving the heat diffusion problem a quantitative formulation for the bubble growth problem is obtained.

Mikic et al.[9]

To predict the bubble growth rate during the inertia controlled phase, Mikic et al.[9] equated the work done by the bubble on the liquid to the total kinetic energy of the liquid due to bubble growth. This resulted in the equation:

$$\left(\frac{dR}{dt}\right)^2 = A^2\frac{T_v - T_{sat}}{\Delta T} \tag{7}$$

Where $\Delta T = T_\infty - T_{sat}$ and $A = \left(\frac{bh_{fg}\rho_v\Delta T}{\rho_l T_{sat}}\right)^{\frac{1}{2}}$

Plesset and Zwick [7] developed an equation for bubble growth in thermally controlled phase for a given liquid superheat and is given by Eq. 8,

$$\frac{dR}{dt} = \frac{1}{2}\frac{B}{\sqrt{t}}\left(\frac{T_\infty - T_v}{\Delta T}\right) \tag{8}$$

Where $B = \left(\frac{12}{\pi}a_1\right)^{\frac{1}{2}} Ja$ and $Ja = \frac{\Delta T c_l \rho_l}{h_{fg}\rho_v}$

Combining the bubble growth equations given in Eq. 7 and Eq. 8, Mikic obtained an equation describing bubble growth for both the phases and is given by,

$$\frac{dR^+}{dt^+} = (t^+ + 1)^{\frac{1}{2}} - (t^+)^{\frac{1}{2}} \tag{9}$$

Where R^+ and t^+ are non-dimensional terms which describe radius and time respectively and are given by $R^+ = \frac{AR}{B^2}$ and $t^+ = \frac{A^2 t}{B^2}$

Integrating Eq. 9, the following relation was obtained,

$$R^+ = \frac{2}{3}\left((t^+ + 1)^{\frac{3}{2}} - (t^+)^{\frac{3}{2}}\right) \tag{10}$$

The model proposed by Mikic et al. accurately predicts bubble growth under various conditions and is widely used. Since the bubble radius and time are expressed in non-dimensional terms, the bubble growth equation can be applied to liquids other than water as well. The addition of the shape factor term also helps predict bubble growth on a heated surface and not just in an infinite uniformly heated liquid.

2.4 Surface enhancements

Open Microchannels

While microchannels were used earlier for flow boiling enhancement, Cooke and Kandlikar [10][11] first used open microchannels for pool boiling of water at atmospheric pressure. They showed that apart from performance enhancement due to the increase in surface area, microchannels also improved surface wetting and liquid circulation. High speed images obtained showed that the bubble nucleates at the base of the microchannel and migrates to the top of the microchannel before it grows. Figure 4 shows the growth of a bubble on a microchannel and liquid circulation inside the channels due to bubble growth.

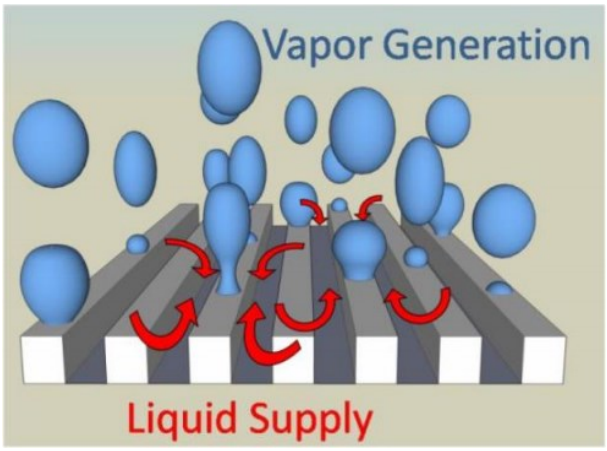

Figure 4: Boiling mechanism on open microchannel surface as proposed by Cooke and Kandlikar [10]

Surface enhancements: Porous surfaces

A significant amount of research was previously performed for developing porous surfaces to enhance boiling. Many mechanisms have been proposed for boiling in a porous medium. Wang et al. [12] proposed that the pores act as nucleation sites and since the density of these sites in a porous surface is significantly higher than that on a plain surface, more nucleation sites are active

for a given wall superheat and hence boiling performance increases. Bergels and Chyu [13] suggested that there are preferred passages through which the vapor formed inside the porous medium escapes. The passages surrounding these escape channels supply water to the nucleation site. Cieslinsk [14] suggested that CHF is reached when rate of generation of vapor exceeds the rate at which the vapor escapes from the escape channels.

Surface enhancements: Nanoscale enhancements

Nanoscale enhancements have been used to improve properties of the surface such as wettablity and thermal conductivity to elevate the boiling performances of the surface. Yao et al [15] coated the surface with nanowires in order to reduce the contact angle of the liquid on the surface. Betz et al. [16] studied the effect of combining superhydrophobic and superhydrophilic patterns on the boiling performance of a surfaces.

2.5 Evaporation momentum force

Evaporation momentum force is a force experienced at a liquid vapor interface where phase change occurs due to the difference in the densities of liquid and vapor. Like the thrust experienced by a rocket due to sudden expansion of the exhaust gasses, a bubble also experiences an outward force when liquid evaporates at the interface to form vapor. Due to the difference in the densities of the liquid and the vapor, the velocity of vapor after evaporation is significantly higher than the velocity of the liquid. The increase in momentum results in a reaction in the opposite direction. In case of a bubble, due to evaporation at the liquid-bubble interface evaporation momentum force pushes the bubble outwards. The magnitude of the force experienced depends on the properties of both the liquid and the vapor and rate of evaporation across the interface.

Evaporation Momentum Force (EMF) was initially studied by Palmer [17]. During bubble growth, EMF pushes the bubble outwards in all directions but has no net effect on the displacement of the bubble as the forces in the opposite direction cancel out. Kandlikar [18] and Nikolayev et al [19] postulated that evaporation momentum force is the driving force behind boiling crisis and that critical heat flux is reached when evaporation momentum force on a bubble overcomes forces which resist bubble growth such as surface tension and gravitational force. Nikolayev [19] expressed evaporation momentum pressure (EMP) as a function of mass flux at the bubble interface as shown in Eq. 11.

$$EMP = \eta^2(\rho_v^{-1} - \rho_l^{-1}) \tag{11}$$

Where η is the evaporation mass flux, and ρ_l and ρ_v liquid and vapor densities respectively.

Effect of Evaporation momentum force on CHF

Kandlikar [18] hypothesized that CHF is reached when the net evaporation momentum force on a bubble is greater than the sum of the surface tension force and the force due to the liquid pressure. Fig. 5 shows the forces acting on the bubble in the horizontal direction.

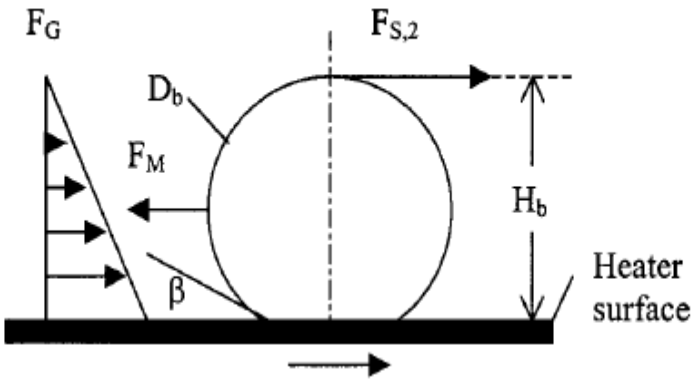

Figure 5: Forces acting on a bubble in the horizontal direction[18]

The horizontal component of evaporation momentum force was expressed as a function of interfacial heat flux and cross sectional area of the bubble as shown in Eq. 12.

$$F_M = \frac{q_I^{''} H_b W}{h_{fg}} \frac{q_I^{''}}{h_{fg}} \frac{1}{\rho_g} = \left(\frac{q_I^{''}}{h_{fg}}\right)^2 \frac{1}{\rho_g} H_b \tag{12}$$

Where $q_I^{''}$ is the interfacial heat flux, h_{fg} is the latent heat of vaporization, H_b is the cross-sectional height and W is the width of the bubble. The width of the bubble was taken as unity and the height of the bubble was a function of contact angle and bubble diameter and was given by,

$$H_b = \frac{D_b}{2}(1 + cos\theta_c) \tag{13}$$

Where D_b is the bubble diameter. The heat flux at the interface is the average heat flux during growth of the bubble from nucleation to departure. The heat flux was derived by considering the interface to be a cylinder with diameter $\frac{D_{avg}}{2}$. Where D_{avg} is the average diameter as the bubble grows and was taken to be $\frac{D_b}{2}$. The area of influence of each bubble is assumed to be twice the bubble diameter. The interfacial heat flux as a function of incident heat flux was expressed as:

$$q_I^{''} = \frac{16q^{''}}{1+\cos\theta_c} \tag{14}$$

When the CHF is reached it was assumed that the evaporation momentum force is greater than the sum of the surface tension forces and the gravitational force. Therefore, the force balance at the interface is given by:

$$F_M = F_{s1} + F_{s2} + F_G \tag{15}$$

Where F_M is the evaporation momentum force, F_s is the surface tension force and F_G is the force due the weight of the liquid. Equating the above forces an expression for CHF was arrived at which closely matches the experimental data. Figure 6 shows the experimental and predicted values of critical heat flux at different pressures for distilled water. The predicted values closely match the experimental results.

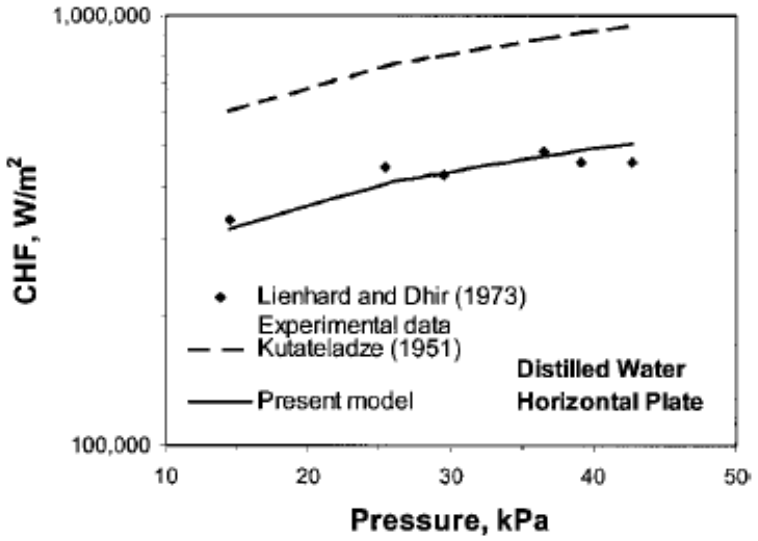

Figure 6: Experimental and predicted values of CHF for distilled water [18]

Lin et al. [20] estimated the magnitude of evaporation momentum force acting on a bubble in a microchannel and suggested that the magnitude of evaporation momentum force on a bubble averaged over its surface is insignificant compared to the shear force experienced by the bubble and the surface tension force on a bubble and hence was not able to elongate a bubble growing in a microchannel. The authors considered the interfacial heat flux to be equal to the incident heat flux.

Contoured fins

For a bubble on a flat horizontal surface, the evaporation momentum force in the horizontal direction is symmetric along the vertical axis and hence the net horizontal force on the bubble is zero. But when a bubble is subjected to an asymmetric temperature distribution, the force on the hotter side of the bubble is greater than the cooler side and hence the bubble experiences a net force towards the hotter side. Figure 7 a) shows the bubble subjected to an asymmetric temperature distribution and the resulting evaporation momentum force experienced by the bubble. Such a condition may be experienced by a bubble nucleating at the base of a fin as shown in Fig. 7 b). Since the temperature on the fin is lower than that on the heater surface, the rate of evaporation near the fin is much lower than that near the heater surface. The resultant evaporation momentum force tends to pushes the bubble away from the fin.

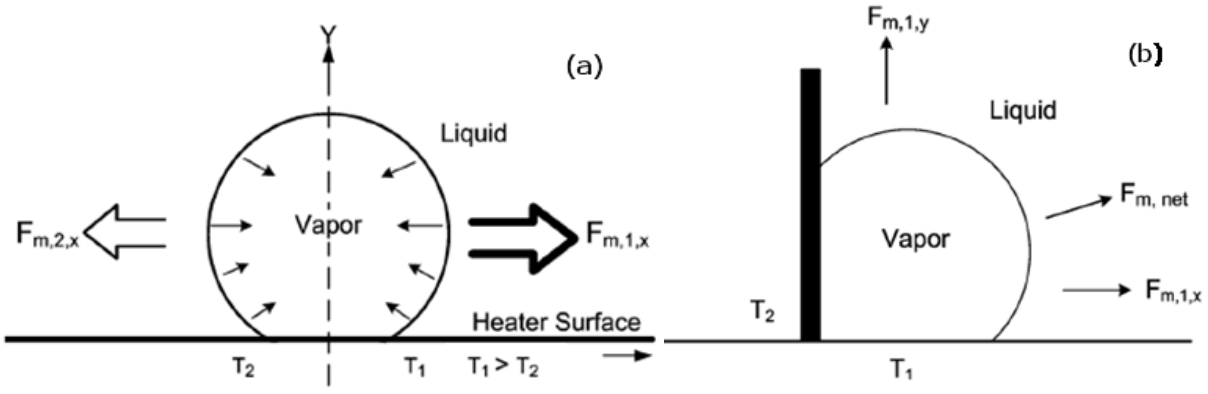

Figure 7 a) schematic of bubble under an asymmetric temperature field b) Schematic of a bubble nucleating at the base of a fin [21]

Kandlikar [21] proposed that this mechanism can be used to control the horizontal trajectory of the bubble and hence establish separate liquid and vapor pathways during boiling. The proposed model had a contoured fin with an artificial nucleation site at the base of the fin as shown in Fig.

8. As the bubble moves away from the fin, a separate pathway for the liquid and vapor is created which greatly increases the boiling performance.

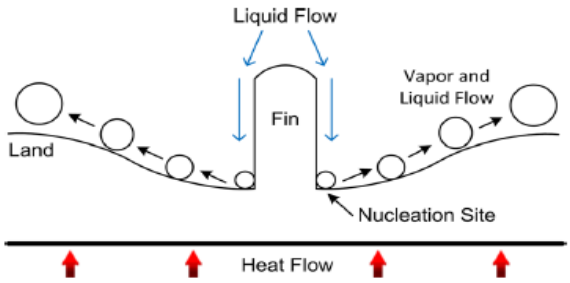

Figure 8: Schematic of the contoured fin with depicting independent liquid and vapor pathways[21]

Figure 9 shows the pool boiling curve obtained using contoured fin compared to a boiling curve for a plain chip. The contoured fin showed a heat transfer coefficient of 629,000 W/m^{2}K and CHF of 3MW/m^2.

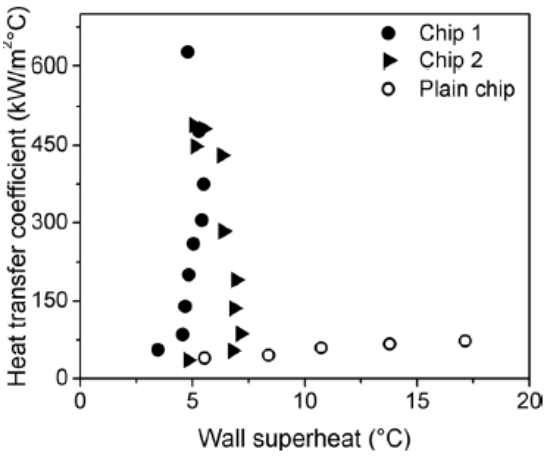

Figure 9: Plot showing the heat transfer coefficient obtained with the chip using the contoured surface shown in Fig.7 [21]

3.0 Objectives

Based on the literature review, it is seen that there are indications that the evaporation momentum force modifies the bubble growth and bubble trajectory. To understand the underlying mechanism further, a detailed theoretical study and visualization of bubble trajectory is proposed. The specific objectives of the present study are:

- Obtain a theoretical model to predict bubble growth rate by modifying existing bubble growth equations to consider the effect of evaporation momentum force.
- Determine the distribution of evaporation momentum force on the surface of a bubble.
- Arrive at a first order approximation of the evaporation momentum force acting on a bubble subjected to asymmetric temperature distribution.
- Predict the horizontal displacement of a bubble subjected to asymmetric temperature distribution as a result of evaporation momentum force.
- Study the effect of various liquid temperature profiles on bubble displacement.
- Visualize the effect of evaporation momentum force on an asymmetrically heated bubble.

4.0 Model

4.1 Expression for EMP

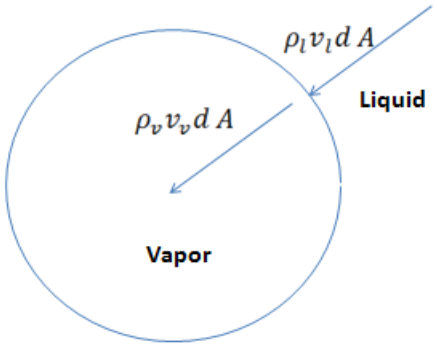

Figure 10: Schematic showing liquid and vapor flow across a bubble interface

Figure 10 shows a schematic of a bubble along with the relative velocities of liquid approaching the bubble and vapor leaving the interface. The liquid approaches the interface with a velocity, v_l relative to the interface and evaporates at the interface. The resultant vapor leaves the interface with a relative velocity, v_v. By applying mass balance across the interface,

$$\rho_l v_l dA = \rho_v v_v dA \tag{16}$$

Where *dA* is the area across which evaporation takes place. Due to the difference in liquid and vapor phase densities, the velocity of the vapor leaving the surface is much greater than the velocity of the approaching liquid. The increase in velocity causes an increase in momentum of the evaporating mass across the interface. Due to the increase in momentum at the interface, the interface experiences a reaction in the opposite direction and this force is referred to as evaporation momentum force. Equation 17 a) gives an expression for evaporation momentum pressure in terms of mass flow rate across the interface. In Equation 17 b) the mass flow rate is expressed in terms of bubble growth rate, $\dot{R}$.

$$EMP = \frac{EMF}{Area} = \frac{\dot{m}(v_v - v_l)}{4\pi R^2} \tag{17a}$$

$$EMP = \frac{4\pi R^2 \dot{R}\rho_v}{4\pi R^2} v_l \left(\frac{v_v}{v_l} - 1\right) \tag{17b}$$

From Eq. 16, the velocity ratio in Eq. 17 b) can be written in terms of liquid and vapor densities and liquid velocity can be written in terms of bubble growth rate. Eq. 17 b) can therefore be written as:

$$EMP = \dot{R}\rho_v \left(\frac{\dot{R}\rho_v}{\rho_l}\right)\left(\frac{\rho_l}{\rho_v} - 1\right) \tag{18}$$

Assuming $\left(\frac{\rho_l}{\rho_v} - 1\right) \approx \frac{\rho_l}{\rho_v}$, the final expression for evaporation momentum pressure can be written as:

$$EMP \approx \dot{R}^2 \rho_v \tag{19}$$

4.2 Effect of EMF on bubble growth

Bubble growth rate using modified Rayleigh Equation

The bubble growth rate is highest during the inertial phase of growth when the radius of the bubble is small. Therefore, evaporation momentum pressure experienced by the bubble is greatest during the initial phase of bubble growth. Since Rayleigh-Plesset equation can be used to predict bubble growth rate during inertia controlled phase, it can be used to determine the effect of evaporation momentum force on bubble growth.

Equation 5 gives the pressures acting at the bubble interface as considered by Rayleigh [6]. To evaluate the effect of evaporation momentum force on bubble growth, Eq. 5 is modified to account for evaporation momentum pressure. The modified expression is given by Eq. 20:

$$P(R) = -\frac{4\mu_l}{R}\frac{dR}{dt} - \frac{2\sigma}{R} + P_v + \dot{R}^2\rho_v \tag{20}$$

Solving the Navier-Stokes equation, given in Eq. 4, using Eq. 20 as boundary condition, an expression for bubble growth rate in terms of pressure difference across the interface, which accounts for evaporation momentum force is obtained and is given by Eq. 21:

$$\frac{P_v - P_l}{\rho_l} = R\frac{d^2R}{dt^2} + \frac{3}{2}\left(\frac{dR}{dt}\right)^2 + \frac{4\vartheta_l}{R}\frac{dR}{dt} + \frac{2\sigma}{\rho_l R} - \frac{\dot{R}^2\rho_v}{\rho_l} \tag{21}$$

Bubble growth rate using modified Mikic model

To predict bubble growth rate in the inertial phase, Mikic et al.[9] equated the kinetic energy of the liquid around the bubble to the work done by the bubble on the liquid. The total kinetic energy (K.E) of the liquid at any instant was expressed as,

$$K.E. = \frac{1}{2}\rho_l \int_R^\infty u^2 dv \tag{22}$$

$$= 2\pi\rho_l(\frac{dR}{dt})^2 R^3$$

Where *u* is the local velocity of the liquid. Work, *W,* done by the bubble on the liquid was expressed as the work done due to the pressure difference across the interface. The effect of evaporation momentum force on bubble growth is considered by adding the work done on the liquid due to evaporation momentum force and the final expression for work done by the bubble is modified to,

$$W = 4\pi \int_0^R (P_v - P_\infty) R^2 dR + 4\pi \int_0^R \left(\dot{R}^2 \rho_v\right) R^2 dR$$

$$W = \frac{4}{3}\pi R^3 ((P_v - P_l) + \dot{R}^2 \rho_v) \tag{23}$$

Mikic et al.[9] assumed that all the kinetic energy of the liquid is due to bubble growth and hence by equating Eq. 22 and Eq. 23 the following expression for bubble growth rate is obtained:

$$\dot{R}^2 = \frac{\frac{2}{3}((P_v - P_l)}{\left(\rho_l - \frac{2}{3}\rho_v\right)} \tag{24}$$

The Clausius-Clayeyron relation between pressure and temperature was used to express the pressure difference across the bubble in terms of temperature difference. Equation 24 can therefore be written as,

$$\dot{R}^2 = \frac{\frac{2}{3} T_v - T_{sat}}{\left(\rho_l - \frac{2}{3}\rho_v\right) T_{sat}} \tag{25}$$

This is similar to the expression derived by Mikic [9]. The effect of evaporation momentum on bubble growth is considered by modifying the parameter '*A*' defined by Mikic [9] to

$$A = \left(b \frac{h_{fg} \rho_v \Delta T}{(\rho_l - b\rho_v) T_{sat}}\right)^{\frac{1}{2}} \tag{26}$$

Where *b* is a parameter defined by Mikic [9] called shape factor and is 2/3 for a spherical bubble and $\pi/7$ for a bubble on a horizontal surface. Since evaporation momentum pressure reduces significantly in the thermally controlled phase, the parameter 'B' used by Mikic [9] is not modified. Hence in the modified expression, the parameter 'A' used to evaluate the non-dimensional variables R^+ and t^+ is changed while the relation between the non-dimensional variables is not modified.

4.3 Assumptions

The bubble growth model proposed by Mikic et al. [9] was used to predict bubble growth rate for the rest of the work. All the assumptions made by Mikic are applicable for the current work. To model the effect of evaporation momentum force on the bubble, the following additional assumptions are made:

- Boundary layer thickness is a function of bubble diameter
- Rate of evaporation is proportional to the liquid superheat
- A bubble in an asymmetric temperature field is assumed to have two distinct temperature fields.

These assumptions and approximations are made to simplify the model and will be explained further in later sections.

4.4 Effect of Temperature distribution

Consider a bubble nucleating on a heater surface. A thermal boundary layer of thickness δ develops on the heater. Inside the boundary layer, temperature of the liquid closer to the heater is greater than the temperature of the liquid further away from the heater. In the initial stages of bubble growth, the height of the bubble is less than the thickness of the boundary layer and hence evaporation takes place throughout the surface of the bubble but is greater towards the heater. As the bubble outgrows the boundary layer, evaporation takes place only within the boundary layer and no evaporation is experienced outside the boundary layer. The rate of evaporation at the interface is highest near the heater surface and reduces with distance from the heater. Figure 11 shows a schematic of the distribution of evaporation occurring at the bubble surface.

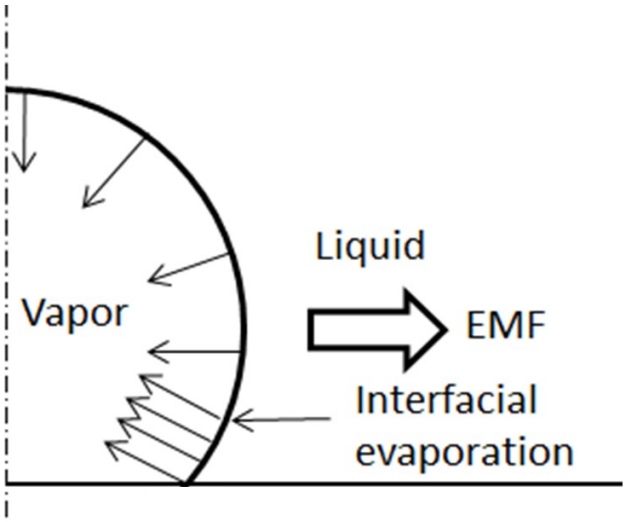

Figure 11: Distribution of evaporation across the interface of the bubble

Mukherjee and Kandlikar [22] simulated boiling on a heated surface and showed that the rate of evaporation observed at the bottom of the bubble is greater than that seen at the top of the bubble. Figure 12 shows a vector plot of the liquid velocities at an instant during bubble growth. As a bubble grows the liquid surrounding the bubble is pushed outwards, however the liquid near the base of the bubble is seen to move towards the bubble. This is due to the high rate of evaporation near the base of the bubble which causes the surrounding liqud to move towards the bubble. Since the rate of evaporation is insignificent at the top of the bubble, the liquid is pushed away from the bubble.

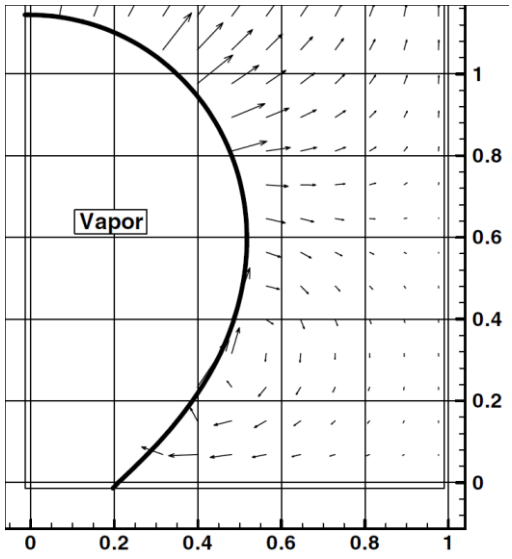

Figure 12: Vector plot showing liquid velocities during bubble growth [22]

Evaporation momentum pressure, as described by Eq. 11 is proportional to the square of the mass flux across the interface. If most of the evaporation occurs at the bottom half of the bubble the mass flux at the bottom half is over two times the mass flux in case of uniformly distributed evaporation. Since EMP is proportional to the square of the mass flux, the average mass flux cannot be considered and the distribution of mass flux needs to be accounted for.4.5 EMF for non-uniform temperature field.

To determine the evaporation momentum force experienced by a bubble under a non-uniform temperature field a correlation between liquid superheat and rate of evaporation is required. Assuming the local rate of evaporation at the interface is proportional to the local liquid superheat, mass flux across the interface at a given location is given by Eq. 27.

$$\eta = c\Delta T \tag{27}$$

Where c is the coefficient of proportionality and ΔT is the local liquid superheat. The local liquid superheat depends on the temperature of the heater surface, thickness of the boundary layer and the temperature distribution in the boundary layer.

Figure 13 shows the schematic of the bubble along with the various angles considered.

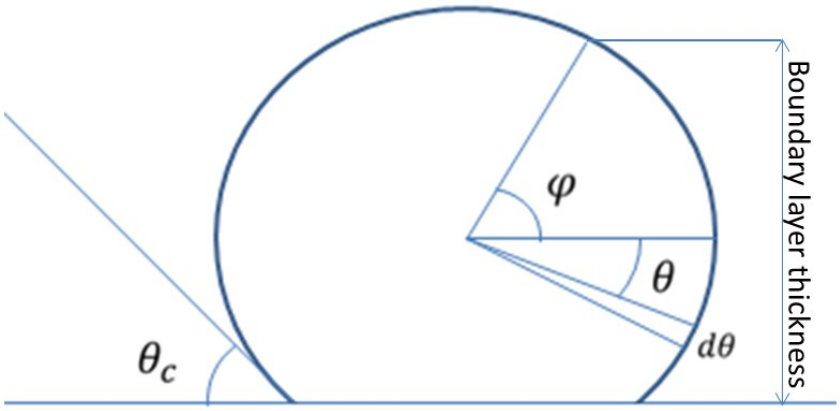

Figure 13: Schematic of bubble showing the angles considered in the model

Here, θ_c is the contact angle of the liquid on the given surface and φ is the angle corresponding to the thermal boundary layer thickness. For saturated boiling, the liquid outside the boundary layer is not superheated and hence no evaporation occurs outside the boundary layer. Therefore, the integral of the mass flux along the bubble interface inside the boundary layer gives the rate of change of mass of the bubble at a given instant. Equation 28 gives the expression for the rate of change of mass of a bubble as a function of local temperature and bubble radius,

$$\dot{m} = 2\int_{-90}^{\varphi} c\Delta T \pi R^2 \cos\theta d\theta \tag{28}$$

Assuming the bubble to be a sphere, the rate of change of mass of the bubble, $\dot{m}$, can be expressed in terms of bubble growth rate, $\dot{R}$ as shown in Eq. 29:

$$\dot{m} = 4\pi R^2 \dot{R} \rho_v \tag{29}$$

From Eq. 27 and Eq. 29 the expression for the constant '*c*' can be written as Eq. 30

$$c = \frac{2\dot{R}\rho_v}{\int_{-90}^{\varphi} \Delta T \cos\theta d\theta} \tag{30}$$

For given temperature profile and bubble growth rate, the constant c and be calculated and hence the local mass flux across the bubble interface can be determined. Once the mass flux across the interface has been determined, the evaporation momentum pressure experienced by the bubble at the interface can be expressed as Eq. 31 and Eq. 32 gives the evaporation momentum force,

$$\mathrm{EMP} = (c\Delta T)^2 \left(\rho_v^{-1} - \rho_l^{-1}\right) \tag{31}$$

$$\mathrm{EMF} = \int_{-90}^{\varphi} (c\Delta T)^2 \left(\rho_v^{-1} - \rho_l^{-1}\right) \pi R^2 \cos\theta d\theta \tag{32}$$

Temperature distribution at bubble interface

The temperature profile of the liquid surrounding the bubble has a significant effect on the magnitude of evaporation momentum force and its distribution on the surface of the bubble. Temperature distribution depends on the heat flux, bubble frequency, waiting time and bubble size. Since the temperature profile around the bubble depends on many factors, evaporation momentum force on a bubble subjected to different temperature conditions are evaluated.

The thickness of the thermal boundary layer and the temperature profile of the liquid in the boundary layer play a critical role in determining the evaporation momentum force experienced by a bubble. For this study, different boundary layer thicknesses and temperature profiles in the boundary layer are modeled to study the resultant EMP experienced by the bubble.

Fixed boundary layer thickness-linear temperature profile

In this case the temperature in the boundary layer is made to vary linearly with height. The thickness of the boundary layer is taken to be *0.6* R_b which corresponds to the geometric center of the bubble. Therefore, the temperature at any point is given by Eq. 33

$$\Delta T = \frac{R \sin\theta}{R \cos\theta_c} T_w \tag{33}$$

Substituting the above relation in Eq. 30 the value of the constant *c* can be found and is given in Eq. 34

$$c = \frac{4\dot{R}\rho_v}{T_w \cos\theta_c} \tag{34}$$

Varying boundary layer thickness- linear temperature profile

Since the thermal boundary layer thickness varies based on the waiting time of the bubble and the heat flux, simulations were carried out assuming the boundary layer to be a variable fraction of the bubble radius. The height of the thermal boundary layer was expressed in terms of φ which is the angle the top of the boundary layer makes with the center of the bubble as shown in Fig. 13. The temperature of the liquid in such a system therefore is given by Eq. 35

$$\Delta T = \frac{\Delta T_W}{\cos\theta_c - \sin\varphi}(\sin\theta - \sin\varphi) \tag{35}$$

Substituting the temperature profile in Eq. 30, an expression for the constant, c, was obtained and is given by Eq. 36

$$c = \frac{4\dot{R}\rho_v}{T_w(\cos\theta_c - \sin\varphi)} \tag{36}$$

Polynomial temperature variation

The liquid around the bubble gets displaced due to bubble grows and the existing temperature profile of the liquid is altered. Mukherjee and Kandlikar [22] simulated bubble growth on a horizontal heater surface and plotted the liquid temperature around the bubble. Figure 14 shows the temperature profile of the liquid around the bubble at a certain point during bubble growth.

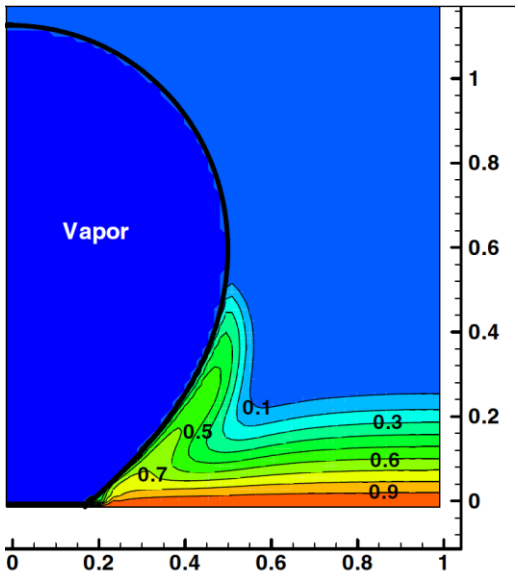

Figure 14: Contour plot showing the temperature of the liquid during bubble growth [22]

Extracting the data from Fig. 14 the temperature profile of the liquid as a fraction of the wall superheat is shown in Fig. 15. The liquid superheat varied cubically with distance from the heater as shown in the Fig. 15.

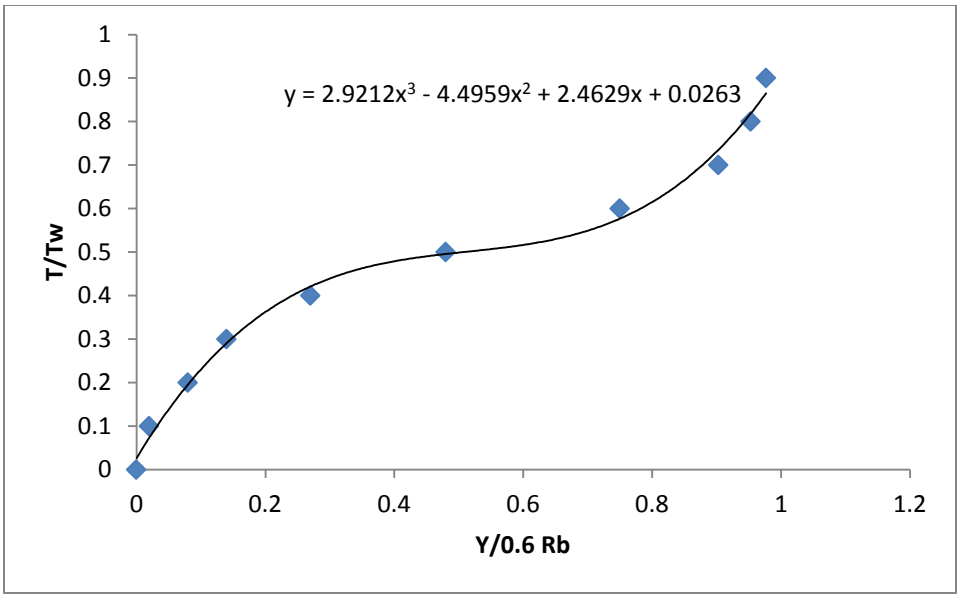

Figure 15: Temperature profile of the liquid shown in Fig 14

Based by the above results, the temperature profile can be represented as a cubic equation given below:

$$\Delta T = \Delta T_w(2.921x^3 - 4.495x^2 + 2.462x + .0263) \tag{37}$$

Where

$$x = \frac{\sin\theta}{\cos\theta_c}$$

For the above temperature profile or any temperature profile represented as a polynomial, the value of the constant c is given by the Eq. 38

$$c = \frac{2\dot{R}\rho_v}{\Delta T cos\,\theta_c\left(\frac{A}{4}+\frac{B}{3}+\frac{C}{2}+D\right)} \tag{38}$$

Where A,B,C and D are the coefficients of the polynomial.

Figure 16 shows the steps taken to calculate the evaporation momentum force experienced by a bubble in the form of a flow chart.

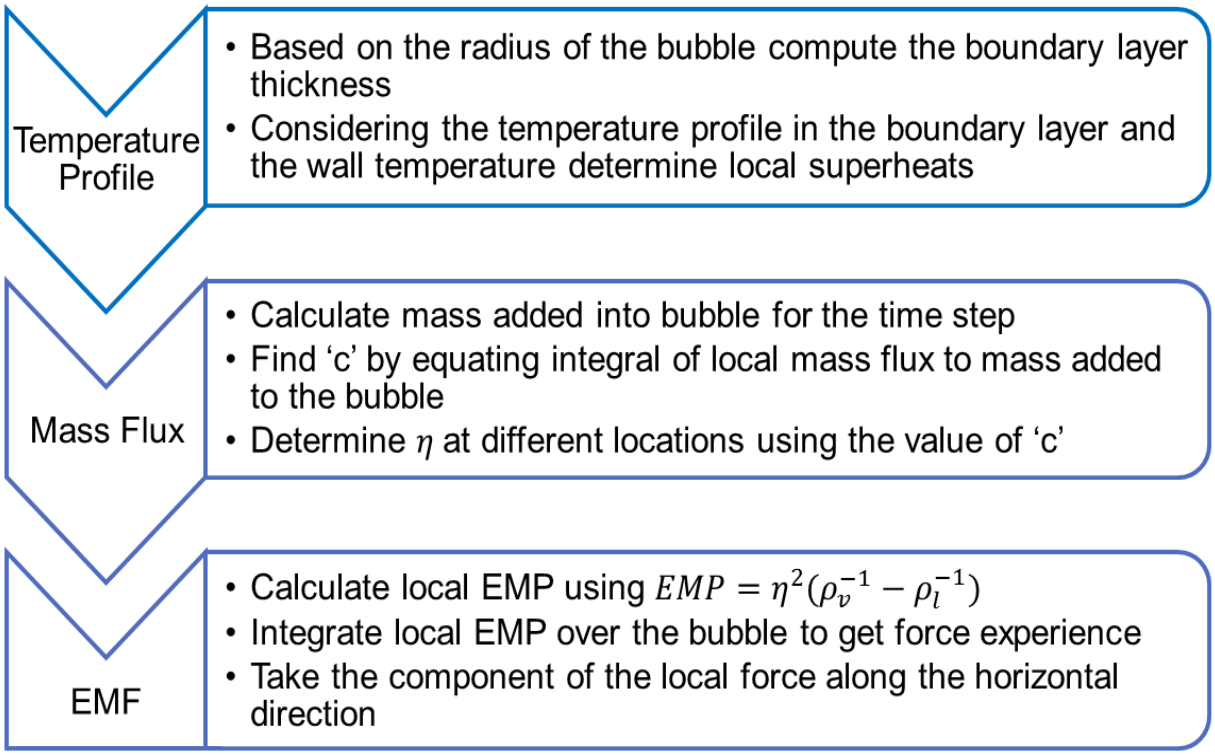

Figure 16: Flow chart of steps to calculate evaporation momentum force

4.6 Asymmetric temperature distribution

Since the evaporation momentum force is dependent on the liquid superheat, a bubble subjected to an asymmetric temperature distribution would experience an unbalanced evaporation momentum force in the horizontal direction. To evaluate the effect of asymmetric temperature distribution, the bubble is assumed to be subjected to two different heater temperatures as shown in Fig. 17.

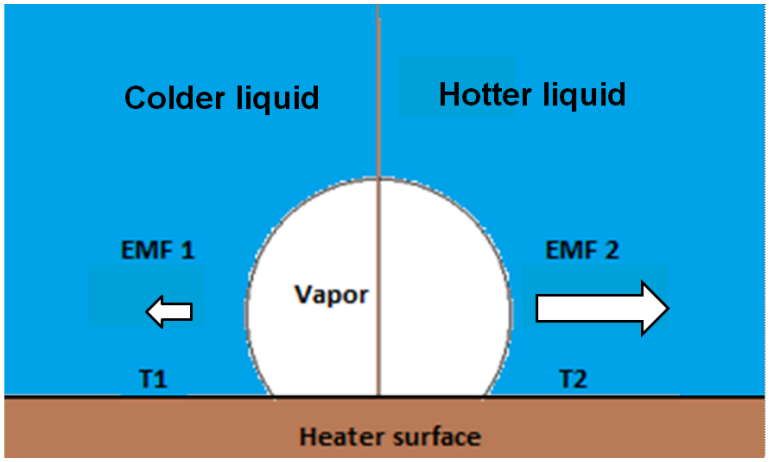

Figure 17: Asymmetric temperature conditions around a bubble

The bubble growth rate in each half is considered to be independent of the other. The bubble growth rate for the halves is computed using Mikic's bubble growth rate equation for the respective wall superheat. The force experienced on each half of the bubble is calculated independently using the respective bubble growth rates. The net force experienced by the bubble is the difference between the forces on each half of the bubble in the horizontal direction.

4.7 Bubble motion

The average radius of a bubble subjected to two different wall superheats is computed by taking the average of the volumes of the two halves of the bubble. To determine the displacement of the bubble, the bubble is assumed to be a ridged spherical body with a cross sectional area, A_b moving through a fluid. As the bubble moves through the liquid it experiences a drag force opposing the motion of the bubble. The expression for drag force on the bubble is given by,

$$F_D = \frac{1}{2}\rho_l V^2 C_D A_b \tag{39}$$

Where V is the velocity of the bubble in the horizontal direction and C_D is the two dimensional coefficient of drag. Sugioka and Komori [23] numerically computed the lift and drag forces experienced by a bubble moving in a liquid. The variation of drag coefficient with respect to Reynolds number for uniform flow is shown in Fig. 18.

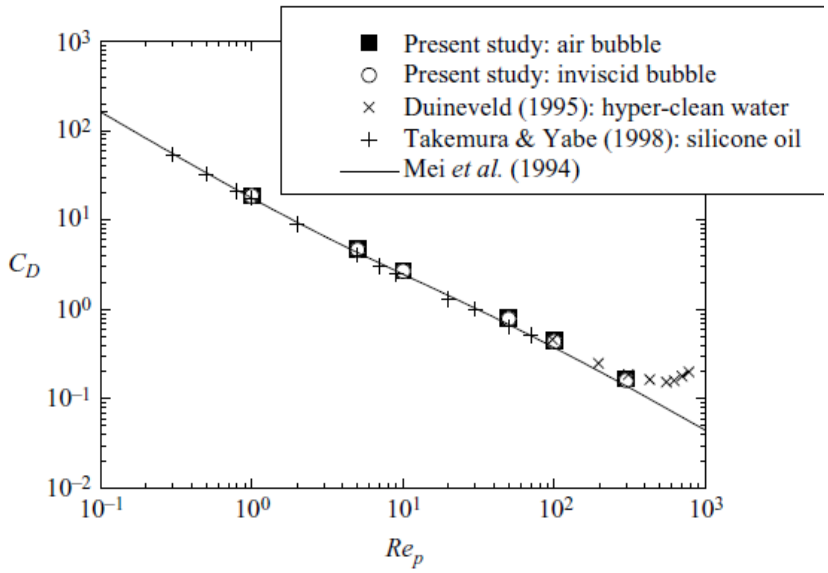

Figure 18:Drag coefficient of a bubble Vs Reynolds number [23]

Since Reynolds number of the system is dependent on the drag force and the drag coefficient is a function of Reynolds number, an iterative process is used to determine the drag coefficient by initially assuming a Reynolds number and varying it until the system is balanced.

Xu et al. [24] visualized the movement of a bubble on a vertical surface to determine the advancing and receding contact angles for a bubble moving along a surface. Figure 19 shows a contact angle of 33^o was observed on the advancing and receding sides.

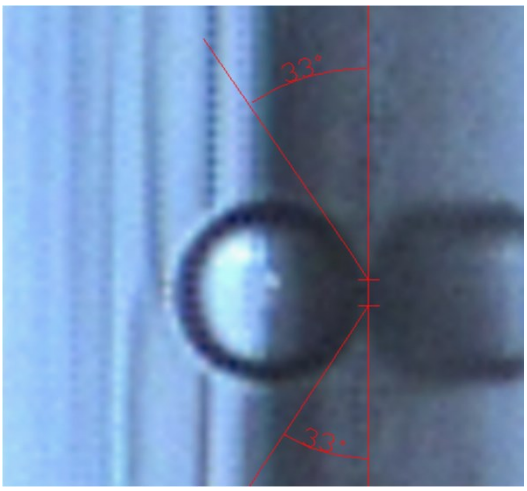

Figure 19: Contact angle of a bubble [24]

Since the contact angles on both sides of the bubble are the same, drag forces due to variation in the horizontal component of surface tension is not considered.

5.0 Experimental Procedure

5.1 Experimental setup

An experimental setup to study and visualize pool boiling of water on a copper surface was used to study the effect of asymmetric temperature distribution on a bubble. The schematic of the experimental test setup is shown in Fig. 20. The main components of the setup are the heater section, the test chip, the quartz glass casing and the liquid reservoir.

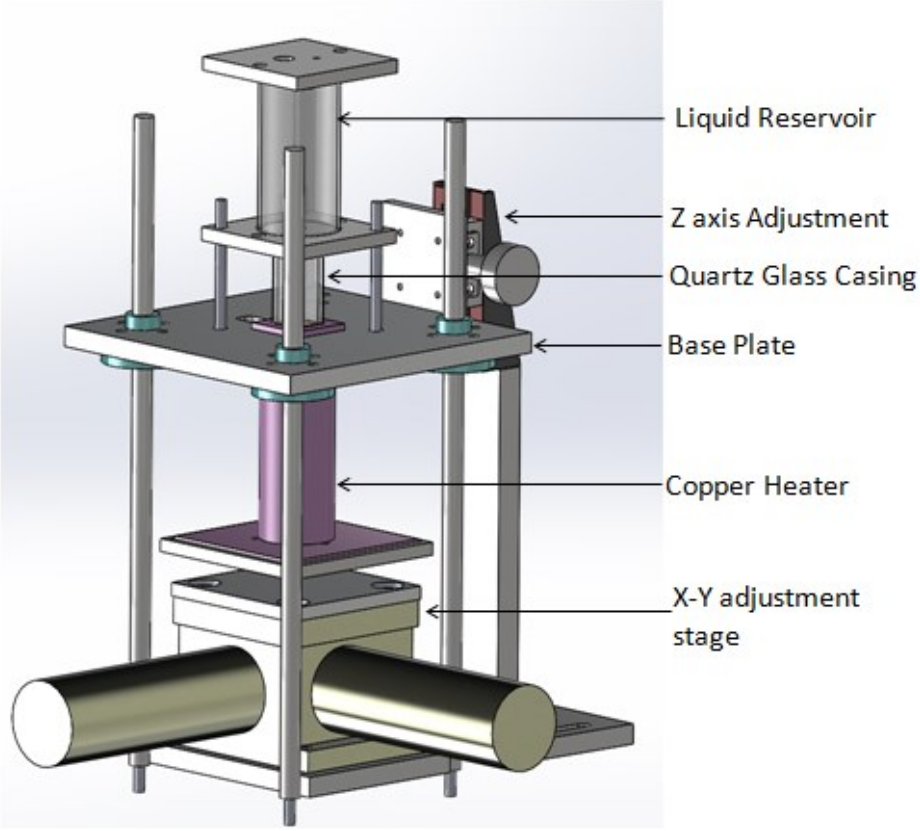

Figure 20: CAD drawing of the test setup

The primary heater consists of a cartridge heater which is inserted in a cylindrical copper shell. The top of the copper heater is in contact with the bottom of the chip. To reduce contact resistance at the interface, a Graphoil® strip is used. The test chip is placed in a ceramic holder.

The liquid on top of the chip is contained using a quartz glass casing. A liquid reservoir is present on top of the glass casing to ensure the surface does not dry out. An auxiliary heater is added so that the bulk liquid is at saturation temperature.

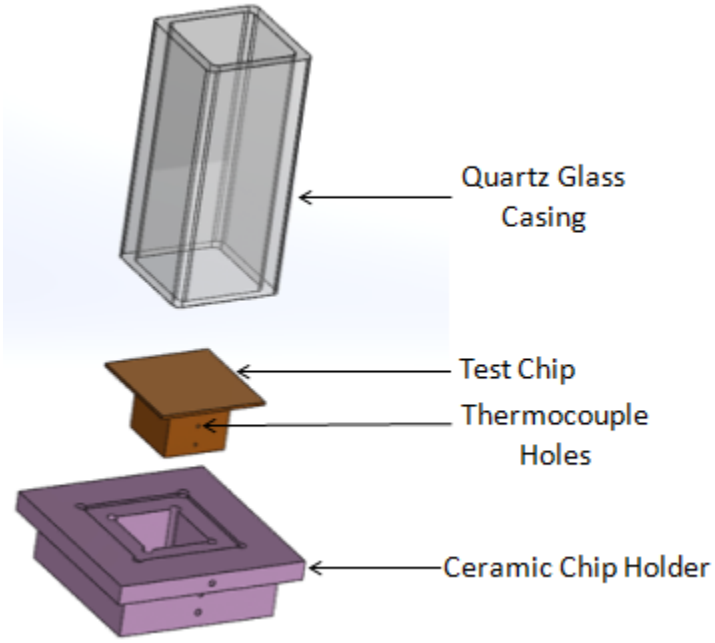

Figure 21: CAD drawing of the test section assembly

The schematic of the test chip and chip holder assembly is shown in Fig. 21. The top of the chip is 17 mm ×17 mm and the total height of the chip is 10.5 mm. The bottom surface of the chip is in contact with the heater while the liquid bath is present on top of the chip. The chip has three holes 0.5 mm in diameter and 3 mm apart on the side. The thermocouples are inserted in these holes and are used to determine the surface temperature and heat flux. The ceramic chip holder is 30.4 mm × 30.4 mm.

The heater assembly is shown in Fig. 22. The copper shell is 26 mm in diameter and 83.82 mm tall. The top of the copper heater is a 10 mm × 10 mm section.

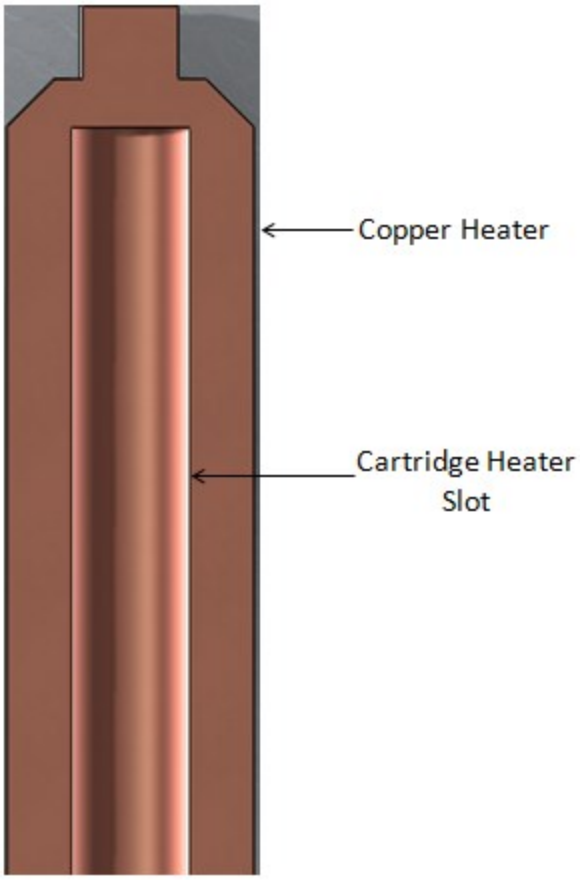

Figure 22: Sectional view of the copper heater

The copper shell has a 12.7 mm hole drilled along its length so that a heat source can be inserted into it. A 1000 W cartridge heater is used for the primary heater and a 200W cartridge heater is inserted into the liquid in the reservoir and functions as the auxiliary heater.

5.2 Experimental procedure

The primary and the auxiliary heaters were powered by DC power sources. The voltage of the current provided was changed to regulate the power input to the heaters. The voltage is maintained till the system reaches steady state before the data is recorded and the visuals are taken. After obtaining visuals of trajectory of the bubble, the voltage is increased till the surface

temperature increases by 1-2^{o}C. This procedure was followed till visualization of bubbles was no longer possible.

5.3 Data acquisition

Data from the setup is acquired through 4 K-type thermocouples. Three thermocouples T1, T2 and T3 are inserted at the bottom of the chip and are spaced 3 mm apart. The fourth thermocouple is inserted from the top of the setup and is used to measure the temperature of the liquid. The thermocouples were connected to a NI-9211 module which in turn was connected to the computer using a NI cDAQ- 9172 chassis. A LabVIEW Virtual instrument (VI) was created to record the temperature readings. Using the data from the four thermocouples, the heat flux and surface temperature at the chip was computed.

5.4 Test section

The test section is a flat copper chip which has been polished to under 0.5 micron roughness. Figure 23 a) shows a schematic of the test section and Fig 23 b) shows an image of the test section as used in the experiment.

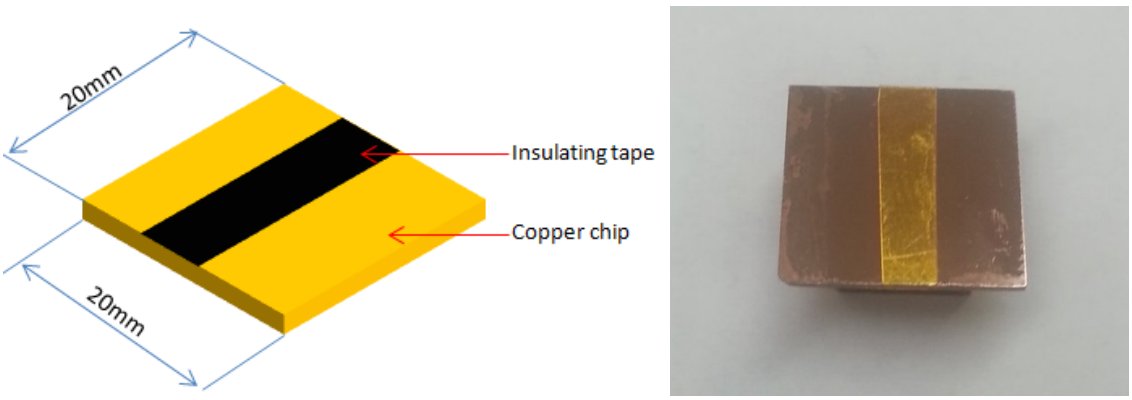

Figure 23 a): Schematic of the test chip 23 b) image of the test chip

A narrow strip of Kaptan® tape was placed over the center of the heater as shown in Fig 23 b). Kaptan tapes are made from Kaptan ® HN film with a silicone adhesive on one side of the film. These tapes can be used at temperatures as high as 260^{o}C without the adhesive giving way or the tape burning. Since the tape is a poor conductor of heat the liquid on top of the tape is at a lower temperature than the liquid on top of the copper surface. Therefore, when a bubble nucleates at the edge of the tape one side of the bubble will be exposed to liquid at a higher temperature than the other side. Since a bubble nucleating at the edge of the tape is subjected to an asymmetric temperature field, evaporation momentum force on the side of the bubble near the tape will be less than the force experienced on the other side.

Chip polishing

In order to obtain visuals of individual bubbles, the number of nucleation sites present on the heater surface had to be reduced. To reduce the number of cavities on the test chip the surface was first ground then polished. Both the grinding and the polishing were carried out on a polishing wheel on which different grinding and polishing disks were magnetically latched. Three grinding and three polishing jobs were carried out on each chip with each operation progressively reducing the roughness of the surface.

The grinding disks have resin bonded diamond surfaces. The first grinding operation is carried out using Struers MD Piano 220 disk. The number at the end of each disk indicates the grit. All the grinding operations are performed using water as a lubricant. The second grinding disk which was used was Struers MD Piano 500. Finally the last grinding operation is carried out using the Struers MD Piano 1200 grinding disk. At the end of the three grinding operations the surface finish of the test chip is comparable to using the finish obtained using a SiC 1200 grit paper.

The polishing operations were carried out using a polishing cloth and a water based diamond suspension which was used as the abrasive. The first polishing operation was carried out using Struers MD-Plan, a polishing cloth made of coated woven polyester and Struers Plan9, a water based diamond suspension containing diamond particles 9 micron in diameter. For the next polishing operation the polishing cloth, Struers MD-Doc was used, which is made of satin woven acetate, and the abrasive used was Struers Dac3, containing diamond particles which are up to 3 microns in diameter. Finally the MD Floc polishing cloth is used with NapB1 which contains suspended diamond particles less than 1 micron in diameter. After the final polishing operation, the roughness of the surface was measured using a laser confocal microscope and was found to be less than 0.5 microns.

6.0 Results

To quantitatively determine the effects of evaporation momentum force on bubble growth and bubble trajectory, the equations described in the previous section were simulated using MATLAB. The simulations were carried out for water boiling on a horizontal copper surface at atmospheric pressure unless specified otherwise. The values of all the properties for water were taken at 100^{o}C.

6.1 Effect of EMF on bubble growth

The effect of evaporation momentum force on bubble growth using the modified Rayleigh-Plesset equation is first analyzed. Figure 24 shows the percentage change in the bubble radius due to evaporation momentum force during bubble growth.

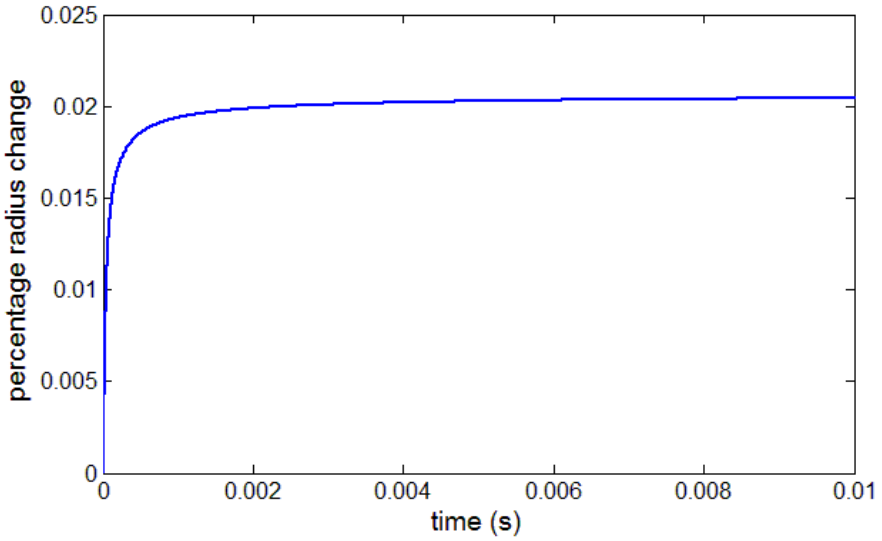

Figure 24: Percentage radius change using modified Rayleigh-Plesset equation

To simulate bubble growth using the Rayleigh-Plesset equation, the pressure difference across the interface at each instant of bubble growth has to be specified. Since this information is not available, the vapor pressure is assumed to be 15% higher than the pressure applied by the forces

resisting bubble growth. This results in a bubble growth rate which is comparable to that obtained using other standard correlations.

The results indicate that the effect of evaporation momentum force on bubble growth for a bubble under uniform temperature conditions is insignificant. This is because the magnitude of forces resisting bubble growth such as surface tension force, viscous force etc. is significantly greater than evaporation momentum force experienced by the bubble at the interface. Most of the percentage increase in the radius of the bubble is observed at initial stage of bubble growth. This is also the stage where the rate of bubble growth is the highest and therefore the evaporation momentum pressure experienced by the bubble is largest.

Figure 25 shows the percentage change in bubble radius as a result of evaporation momentum using the modified Mikic equation. The percentage change in radius is more significant at a higher wall superheat compared to lower wall superheats. This is because evaporation momentum force is greater at higher temperatures due to higher mass flux at the bubble interface.

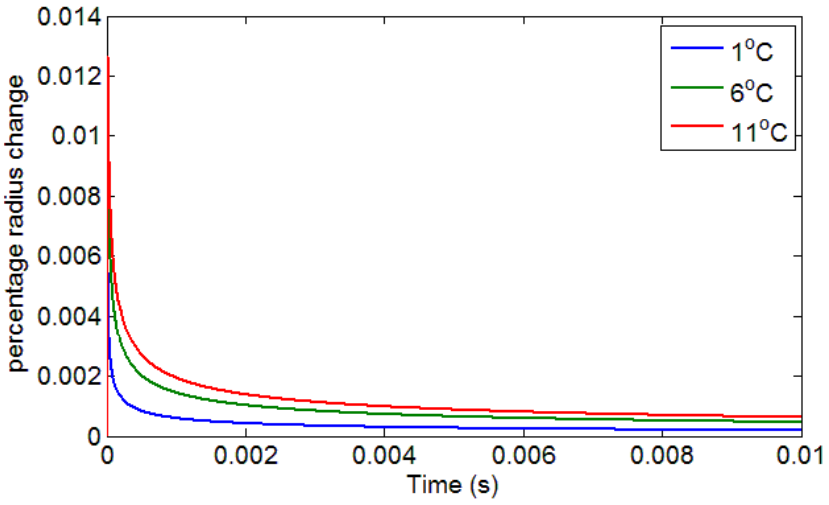

Figure 25: Percentage radius change using modified Mikic's equation

The modified Rayleigh-Plesset Equation shows the percentage change in radius of the bubble due to evaporation momentum force reaches its maximum value of about 0.02% towards the end of the simulation. The modified Mikic equation on the other hand indicates that the effect of evaporation momentum force reduces and reaches its minimum value at the end of the simulation. This is because the Rayleigh-Plesset equation is used to model only the inertial growth phase while Mikic's equation the entire bubble growth. Also, the effect of evaporation momentum force in the thermally controlled phase is ignored in the modified Mikic equation while evaporation momentum force is considered to be applicable throughout bubble growth using modified Rayleigh equation.

From Fig. 24 and Fig. 25 it can be seen that the effect of evaporation momentum force on bubble growth is negligible. Apart from the reasons mentioned earlier this is also because evaporation is assumed to occur uniformly throughout the surface of the bubble in both the models, the mass flux across the interface is lower than the mass flux experienced by a bubble on a heater surface.

6.2 Distribution of EMF and bubble displacement

Evaporation momentum pressure experienced by a bubble in non-uniform temperature fields varies significantly from the force experienced in uniform temperature field. In case of a bubble with $\delta = 0.6\,R_b$ and linear temperature profile inside the boundary layer, the maximum evaporation momentum pressure experienced is 16 times the evaporation momentum pressure experienced by a bubble in a uniformly heated liquid. Figure 26 shows the variation of Evaporation momentum pressure along the height of the bubble for two different temperature profiles. For a temperature profile where $\delta = 0.3R_b$ and linear temperature profile inside the boundary layer the evaporation momentum pressure at the base of the bubble is about 64 times the pressure experienced under uniform temperature distribution.

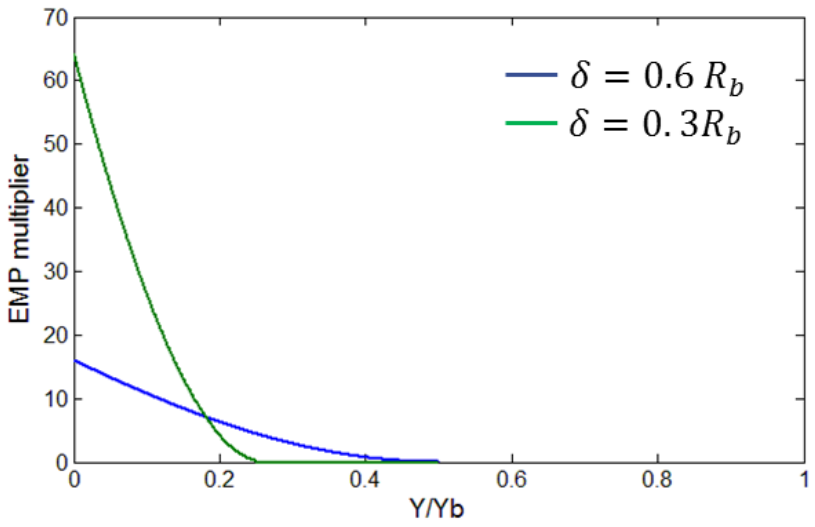

Figure 26: Variation of evaporation momentum pressure along the height of the bubble

The displacement of the bubble due to evaporation momentum force also depends on the temperature profile of the liquid surrounding the bubble. Figure 27 a) shows the displacement of the bubble where $\delta = 0.6\,R_b$ and the temperature profile inside the boundary layer is linear. Figure 27 b) shows the displacement of the bubble compared to the radius of the bubble.

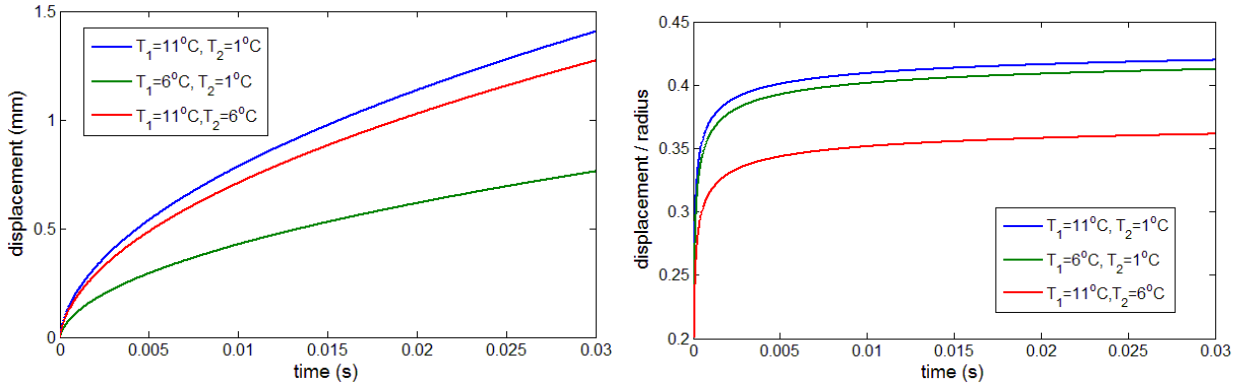

Figure 27 a) Displacement of the bubble subjected to different temperatures where δ =0.6 R_b b) displacement of the bubble as a fraction of bubble radius

The displacement of the bubble is highest when the temperature difference across the bubble is greatest. While higher temperatures lead to larger displacement, displacement of the bubble as a fraction of the radius of the bubble is lower at high temperatures as the radius of the bubble is large and hence the bubble experiences greater drag.

The displacement of the bubble subjected to $\boldsymbol{\delta = 0.3\ R_b}$ and the temperature profile inside the boundary layer is linear is shown in Fig. 28. The evaporation momentum force experienced by the bubble in this case is twice the force experienced when $\boldsymbol{\delta}$ =0.6 R_b yet the displacement experienced by the bubble is only about 40% higher.

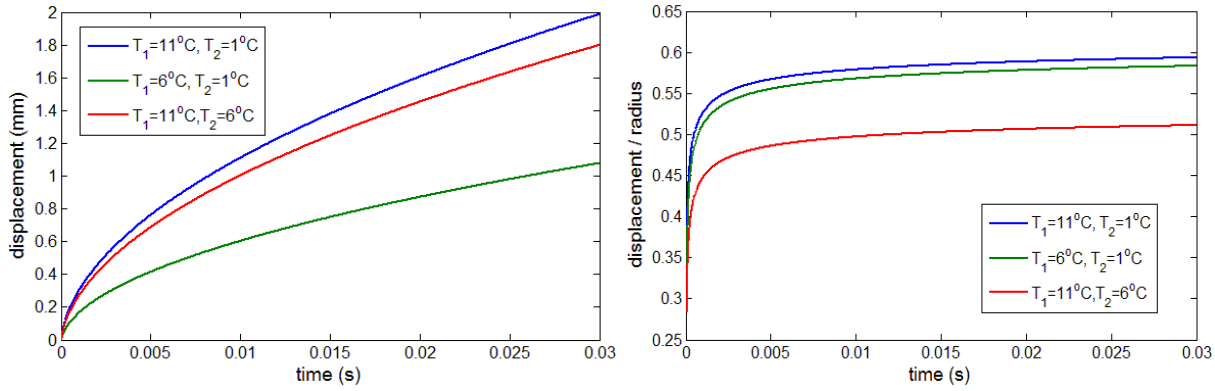

Figure 28 a) Displacement of the bubble subjected to different temperatures where $\boldsymbol{\delta}$ =0.3 R_b b) displacement of the bubble as a fraction of bubble radius

Finally, the displacement of the bubble where the temperature inside the boundary layer varies in a cubic fashion as shown is Eq. 38 is shown is Fig. 29. Despite assuming the boundary layer thickness to be 0.6 R_b, it can be seen that with a cubically varying temperature profile the displacement of the bubble is greater than that with a linearly varying profile as seen in Fig. 27.

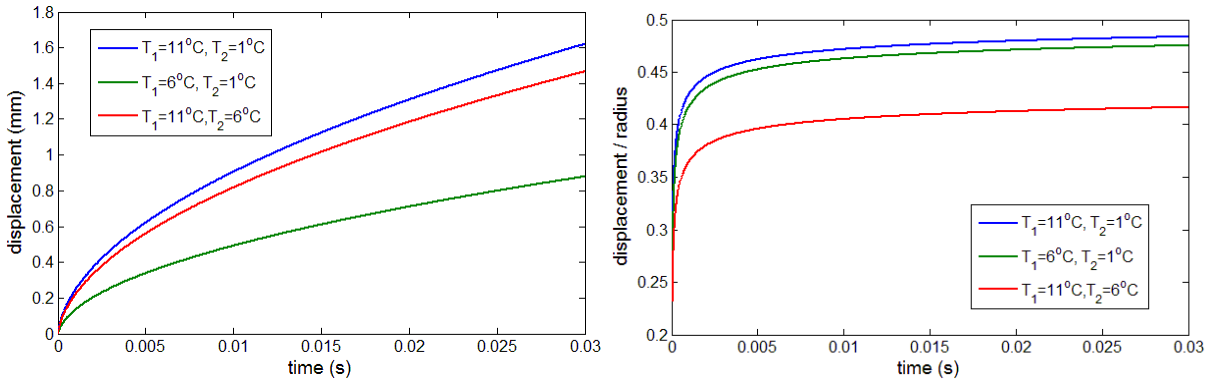

Figure 29 a) Displacement of the bubble subjected to cubically varying temperature profile b) displacement of the bubble as a fraction of bubble radius

From the results shown it is clear that the displacement of the bubble can vary with both the thickness of the boundary layer and the temperature profile in the boundary layer. At heat fluxes near CHF the effect of evaporation momentum force is more pronounced as the rate of evaporation is very high and temperature gradient in the boundary layer is steep thereby altering the distribution of evaporation on the interface.

6.3 Visualization and Comparison

In order to experimentally observe the effect of evaporation momentum force on a bubble, high speed images of a bubble subjected to asymmetric temperature filed was captured. The high speed video was captured using Photron high speed camera and the video was recorded at 10000 frames per second. Fig. 30 shows six frames captured during boiling with a surface temperature of 104 ^{o}C.

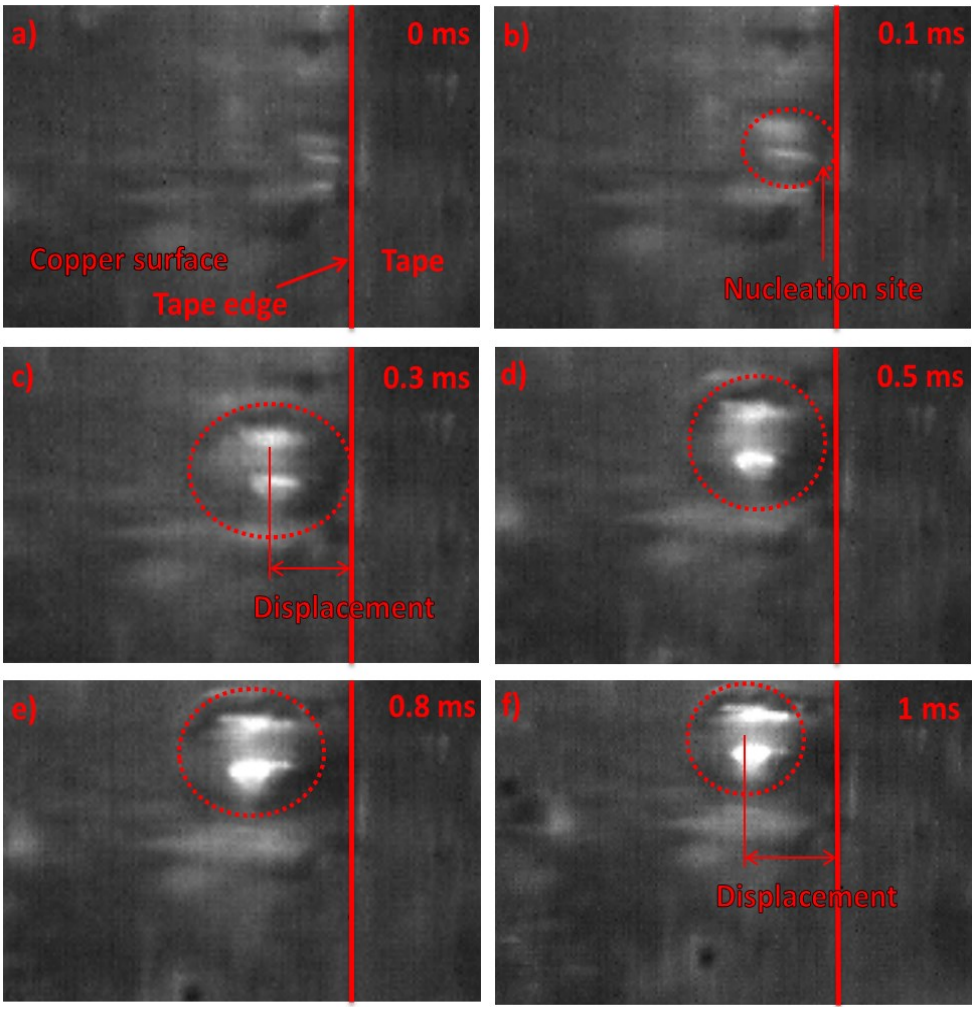

Figure 30 (a-f): Lateral bubble displacement at a surface superheat of 4^{o}C

The images show a bubble shifting to the left due to evaporation momentum pressure. The bubble begins to nucleate at 0 ms in Fig. 30 a) and can be first seen in Fig. 30 b). As the bubble grows, the center of the bubble moves away from the nucleation site as seen in Fig. 30 c) and Fig. 30 d). By 0.8 ms the bubble is completely detached from the tape and continues to move due to inertia of motion. By the time the bubble departs in Fig. 30 f) the bubble has been displaced by a distance greater than its own radius and it continues to move horizontally in the liquid after departure. It was confirmed that the lateral motion of the bubble was not due to liquid motion at the nucleation site by observing a stationary bubble sitting on the top of the tape. The results

from the visualization shows that under an asymmetric temperature field a bubble indeed moves towards the hotter side due to unbalanced evaporation momentum force. Since displacement of the interface has the bubble growth component intrinsic in it, the displacement of the center of the bubble is considered to determine the effect of evaporation momentum force. Figure 31 shows the displacement of the center of the bubble as seen in the visuals and the predicted displacement under different boundary layer conditions.

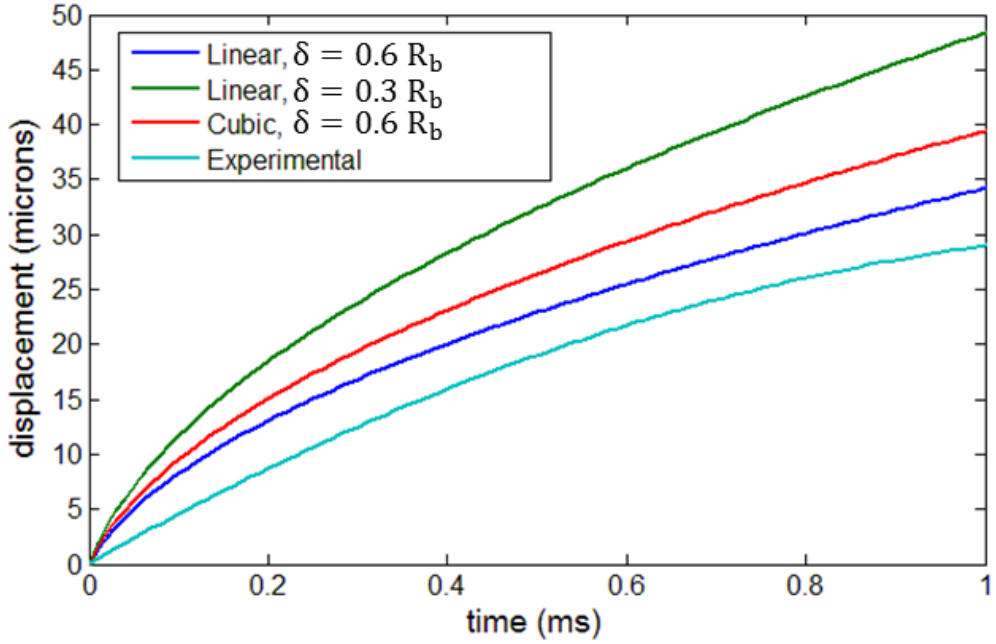

Figure 31: Experimental and predicted bubble displacement

It can be seen from Fig. 31 that the actual displacement and the predicted displacement with $\delta = 0.6\ R_b$ and a linear temperature distribution are in close agreement. At the time of bubble departure the error between the predicted and actual displacement is about 23%. Therefore by choosing the appropriate temperature distribution the displacement of the bubble can be accurately predicted. The wall superheat in the experiments was only 4 °C. At higher wall superheats, the bubble displacement is expected to be significantly more severe.

7.0 Conclusion

The effect of evaporation momentum force on bubble growth and bubble trajectory was theoretically analyzed. Visualization of bubble trajectory was carried out by subjecting a bubble to an asymmetric temperature condition. The following conclusions can be drawn from the results obtained:

i) For a bubble growing in a uniform temperature field, evaporation momentum force is distributed throughout the surface of the bubble and is around two orders of magnitude lower than forces opposing bubble growth. Therefore its effect on bubble growth is insignificant.

ii) Evaporation momentum pressure on a bubble is greatest in the initial stages of bubble growth when the rate of evaporation is high but the area available for evaporation is limited.

iii) Evaporation momentum force on a bubble is greater at higher heat fluxes as the bubble growth time is much lower and hence the mass flux across the interface is significantly greater.

iv) Distribution of evaporation over the surface of the bubble depends on the temperature profile of the liquid surrounding the bubble and since for a bubble nucleating on a heated surface the liquid is hottest at the base of the bubble, most of the evaporation occurs at the bottom half of the bubble.

v) An asymmetric temperature distribution around a bubble causes an imbalance in the evaporation momentum force experienced by the bubble and hence the bubble experiences a net force in the horizontal direction towards the hotter side.

vi) High speed video obtained during boiling shown that the bubble tends to move towards the hotter side during bubble growth and after bubble departure as well.

vii) Experimental data on the displacement of the bubble closely matches the predicted displacement with the simulation for linear temperature profile with $\delta = 0.6\, R_b$ having a 28 % variation with experimental data during bubble departure.

8.0 Future work

The theoretical model developed to predict bubble displacement due to evaporation momentum force can be applied to develop contoured fins like those developed by Kandlikar [21] to enhance boiling performance. The profile of the fins and the spacing between the fins can be determined by better understanding the trajectory followed by the bubble.

The effect of evaporation momentum force on the shape of the interface especially near the contact line remains unknown. Contact angle variation due to the change of shape also needs to be examined. While the visuals of bubble displacement were obtained at a low heat flux the displacement of the bubble at higher heat fluxes needs to be obtained. Numerical simulations using software such as surface evolver or ANSYS can be used to simulate surface deformation as a result of evaporation momentum force. Simulations can also be carried out to predict the magnitude of evaporation momentum force near CHF and its effect on bubble deformation.

9.0 References

[1] B. B. Mikic and W. M. Rohsenow, "A New Correlation of Pool-Boiling Data Including the Effect of Heating Surface Characteristics," *J. Heat Transf.*, vol. 91, no. 2, pp. 245–250, May 1969.

[2] W. M. Rohsenow, "A method of correlating heat transfer data for surface boiling of liquids," *J. Heat Transf.*, vol. 74, p. 969, 1951.

[3] N.R. Snyder and D. K. Edwards, "Summary of conference on bubble dynamics and boiling heat transfer."

[4] M. G. Cooper and A. J. P. Lloyd, "The microlayer in nucleate pool boiling," *Int. J. Heat Mass Transf.*, vol. 12, no. 8, pp. 895–913, Aug. 1969.

[5] J. Kim, "Review of nucleate pool boiling bubble heat transfer mechanisms," *Int. J. Multiph. Flow*, vol. 35, no. 12, pp. 1067–1076, Dec. 2009.

[6] L. Rayleigh, "Pressure due to collapse of bubbles," *Phil Mag*, vol. 94, 1917.

[7] M. S. Plesset and S. A. Zwick, "The Growth of Vapor Bubbles in Superheated Liquids," *J. Appl. Phys.*, vol. 25, no. 4, pp. 493–500, May 2004.

[8] M. S. Plesset, "Dynamics of cavitation bubbles," *Am. Soc. Mech. Eng. -- Trans. -- J. Appl. Mech.*, vol. 16, no. 3, pp. 277–282, 1949.

[9] B. B. Mikic, W. M. Rohsenow, and P. Griffith, "On bubble growth rates," *Int. J. Heat Mass Transf.*, vol. 13, no. 4, pp. 657–666, Apr. 1970.

[10] D. Cooke and S. G. Kandlikar, "Effect of open microchannel geometry on pool boiling enhancement," *Int. J. Heat Mass Transf.*, vol. 55, no. 4, pp. 1004–1013, Jan. 2012.

[11] D. Cooke and S. G. Kandlikar, "Pool Boiling Heat Transfer and Bubble Dynamics Over Plain and Enhanced Microchannels," *J. Heat Transf.*, vol. 133, no. 5, p. 052902, 2011.

[12] X. Wang, Z. Wang, and Q. Chen, “Research on Manufacturing Technology and Heat Transfer Characteristics of Sintered Porous Surface Tubes,” in *Manufacturing Science and Engineering, Pts 1-5*, vol. 97–101, Z. Jiang and C. L. Zhang, Eds. Stafa-Zurich: Trans Tech Publications Ltd, 2010, pp. 1161–1165.

[13] A. Bergles and M. Chyu, “Characteristics of Nucleate Pool Boiling from Porous Metallic Coatings,” *J. Heat Transf.-Trans. Asme*, vol. 104, no. 2, pp. 279–285, 1982.

[14] J. T. Cieilinski, “Nucleate pool boiling on porous metallic coatings,” *Int. Therm. Semin. Part 2*, vol. 25, no. 7, pp. 557–564, 2002.

[15] Z. Yao, Y.-W. Lu, and S. G. Kandlikar, “Direct growth of copper nanowires on a substrate for boiling applications,” *Micro Nano Lett.*, vol. 6, no. 7, p. 563, 2011.

[16] A. R. Betz, J. Jenkins, Chang-Jin Kim, and D. Attinger, “Boiling heat transfer on superhydrophilic, superhydrophobic, and superbiphilic surfaces,” *Int. J. Heat Mass Transf.*, vol. 57, no. 2, pp. 733–41, Feb. 2013.

[17] H. J. Palmer, “The hydrodynamic stability of rapidly evaporating liquids at reduced pressure,” *J. Fluid Mech.*, vol. 75, no. 03, pp. 487–511, 1976.

[18] S. G. Kandlikar, “A Theoretical Model to Predict Pool Boiling CHF Incorporating Effects of Contact Angle and Orientation,” *J. Heat Transf.*, vol. 123, no. 6, pp. 1071–1079, Apr. 2001.

[19] V. S. Nikolayev, D. Chatain, Y. Garrabos, and D. Beysens, “Experimental evidence of the vapor recoil mechanism in the boiling crisis,” *Phys. Rev. Lett.*, vol. 97, no. 18, p. 184503, Nov. 2006.

[20] L. Yin, L. Jia, P. Guan, and F. Liu, “Evaporating momentum force and shear force on meniscuses of elongated bubble in microchannel flow boiling,” *J. Therm. Sci.*, vol. 23, no. 2, pp. 160–168, Apr. 2014.

[21] S. G. Kandlikar, “Controlling bubble motion over heated surface through evaporation momentum force to enhance pool boiling heat transfer,” *Appl. Phys. Lett.*, vol. 102, no. 5, p. 051611, 2013.

[22] A. Mukherjee and S. G. Kandlikar, “Numerical study of single bubbles with dynamic contact angle during nucleate pool boiling,” *Int. J. Heat Mass Transf.*, vol. 50, no. 1–2, pp. 127–138, Jan. 2007.

[23] K.-I. Sugioka and S. Komori, “Drag and lift forces acting on a spherical gas bubble in homogeneous shear liquid flow,” *J. Fluid Mech.*, vol. 629, p. 173, Jun. 2009.

[24] J. Xu, B. Chen, Y. Huang, X. Yan, and D. Yuan, “Experimental visualization of sliding bubble dynamics in a vertical narrow rectangular channel,” *Nucl. Eng. Des.*, vol. 261, pp. 156–164, Aug. 2013.